

1 **JIB-04 has broad-spectrum antiviral activity and inhibits SARS-CoV-2 replication**  
2 **and coronavirus pathogenesis**

3

4 Juhee Son<sup>1,2,\*</sup>, Shimeng Huang<sup>3,\*</sup>, Qiru Zeng<sup>1,\*</sup>, Traci L. Bricker<sup>4</sup>, James Brett Case<sup>4</sup>,  
5 Jinzhu Zhou<sup>3</sup>, Ruochen Zang<sup>1,5</sup>, Zhuoming Liu<sup>1</sup>, Xinjian Chang<sup>3</sup>, Houda H. Harastani<sup>4</sup>, Lu  
6 Chen<sup>6</sup>, Maria Florencia Gomez Castro<sup>1</sup>, Yongxiang Zhao<sup>3</sup>, Hinissan P. Kohio<sup>1</sup>, Gaopeng  
7 Hou<sup>1</sup>, Baochao Fan<sup>3</sup>, Beibei Niu<sup>3</sup>, Rongli Guo<sup>3</sup>, Paul W. Rothlauf<sup>1,7</sup>, Adam L. Bailey<sup>8</sup>, Xin  
8 Wang<sup>5</sup>, Pei-Yong Shi<sup>9</sup>, Elisabeth D. Martinez<sup>10</sup>, Sean P.J. Whelan<sup>1</sup>, Michael S.  
9 Diamond<sup>1,4,8</sup>, Adrianus C.M. Boon<sup>1,4,8</sup>, Bin Li<sup>3,#</sup>, Siyuan Ding<sup>1,#</sup>

10

11 <sup>1</sup>Department of Molecular Microbiology, Washington University School of Medicine, St.  
12 Louis, MO, USA. <sup>2</sup>Program in Molecular Cell Biology, Washington University School of  
13 Medicine, St. Louis, MO, USA. <sup>3</sup>Institute of Veterinary Medicine, Jiangsu Academy of  
14 Agricultural Sciences, Nanjing, China. <sup>4</sup>Department of Medicine, Division of Infectious  
15 Diseases, Washington University School of Medicine, St. Louis, MO, USA. <sup>5</sup>Key  
16 Laboratory of Marine Drugs, Ministry of Education, Ocean University of China, Qingdao,  
17 China. <sup>6</sup>National Center for Advancing Translational Sciences, National Institutes of  
18 Health, Rockville, MD, USA. <sup>7</sup>Program in Virology, Harvard Medical School, Boston, MA,  
19 USA. <sup>8</sup>Department of Pathology and Immunology, Washington University School of  
20 Medicine, St. Louis, MO, USA. <sup>9</sup>Department of Biochemistry and Molecular Biology,  
21 University of Texas Medical Branch, Galveston TX, USA. <sup>10</sup>Department of Pharmacology,  
22 UT Southwestern Medical Center, Dallas, TX 75390, USA.

23

24 \* These authors contributed equally: Juhee Son, Shimeng Huang, Qiru Zeng

25 # Corresponding authors: Bin Li, [libinana@126.com](mailto:libinana@126.com), Siyuan Ding, [siyuan.ding@wustl.edu](mailto:siyuan.ding@wustl.edu)

26

## 27 **Abstract**

28

29 Pathogenic coronaviruses represent a major threat to global public health. Here, using a  
30 recombinant reporter virus-based compound screening approach, we identified several  
31 small-molecule inhibitors that potently block the replication of the newly emerged severe  
32 acute respiratory syndrome virus 2 (SARS-CoV-2). Among them, JIB-04 inhibited SARS-  
33 CoV-2 replication in Vero E6 cells with an EC<sub>50</sub> of 695 nM, with a specificity index of  
34 greater than 1,000. JIB-04 showed *in vitro* antiviral activity in multiple cell types against  
35 several DNA and RNA viruses, including porcine coronavirus transmissible gastroenteritis  
36 virus. In an *in vivo* porcine model of coronavirus infection, administration of JIB-04  
37 reduced virus infection and associated tissue pathology, which resulted in improved  
38 weight gain and survival. These results highlight the potential utility of JIB-04 as an  
39 antiviral agent against SARS-CoV-2 and other viral pathogens.

40

## 41 **INTRODUCTION**

42

43 The coronavirus disease 2019 (COVID-19) pandemic has caused unprecedented global  
44 morbidity, mortality, and socioeconomic destabilization. Thus, there is an urgent unmet  
45 need to develop safe and effective countermeasures to combat the disease beyond  
46 vaccine protection and provide immediate treatment. Multiple efforts are underway to

47 identify candidate drugs that inhibit the replication of severe acute respiratory syndrome  
48 virus 2 (SARS-CoV-2) (Riva *et al.*, 2020; Touret *et al.*, 2020; Dittmar *et al.*, 2021; Heiser  
49 *et al.*, 2020; Mirabelli *et al.*, 2020), the cause of COVID-19 (Wu *et al.*, 2020; Zhou *et al.*,  
50 2020). So far, several small-molecule inhibitors that interfere with SARS-CoV-2 cell entry  
51 have been identified, including transmembrane serine protease inhibitors camostat  
52 (Hoffmann *et al.*, 2020) and nafamostat (Wang *et al.*, 2020a), and endosomal inhibitors  
53 including chloroquine and its derivatives (Wang *et al.*, 2020a), E-64d (Hoffmann *et al.*,  
54 2020), apilimod (Kang *et al.*, 2020), and 25-hydroxycholesterol (Zang *et al.*, 2020a). Drug  
55 screens and structural studies also revealed compounds that target the viral enzymes of  
56 SARS-CoV-2, namely the RNA-dependent RNA polymerase (Yin *et al.*, 2020; Gao *et al.*,  
57 2020; Kirchdoerfer and Ward, 2019; Nguyen *et al.*, 2020; Sheahan *et al.*, 2020) and the  
58 main protease (M<sup>pro</sup>, also known as 3CL<sup>pro</sup>) (Zhang *et al.*, 2020; Dai *et al.*, 2020; Jin *et al.*,  
59 2020; Nguyen *et al.*, 2020). Here, utilizing a fluorescent SARS-CoV-2 virus and an  
60 imaging-based screen approach, we identified several known and previously unknown  
61 antiviral compounds that inhibit SARS-CoV-2 replication.

62

## 63 **RESULTS**

64

65 To identify small molecules with anti-SARS-CoV-2 activity, we performed a screen using  
66 a recombinant SARS-CoV-2 that encoded mNeonGreen as a reporter of infection (Xie *et al.*  
67 *et al.*, 2020) and an in-house collection of ~200 compounds that comprised FDA-approved  
68 drugs, well-defined broad-spectrum antiviral agents, and investigational new drugs. We  
69 identified 157 compounds that had greater antiviral efficacy (>44.8% inhibition) than either

70 chloroquine or remdesivir against SARS-CoV-2 replication in Vero E6 cells (**Fig. 1A** and  
71 **Dataset S1**). One of these drugs was a pan-Jumonji histone demethylase inhibitor 5-  
72 chloro-N-[(E)-[phenyl(pyridin-2-yl)methylidene]amino]pyridin-2-amine (JIB-04 E-isomer)  
73 (Wang *et al.*, 2013) (**Fig. S1A**). We selected JIB-04 (JIB-04 E-isomer, unless noted  
74 otherwise) for further characterization because several histone demethylases were  
75 recently discovered as SARS-CoV-2 host dependency factors (Wei *et al.*, 2021; Wang *et*  
76 *al.*, 2021; Schneider *et al.*, 2021) and JIB-04 has not been reported as an antiviral  
77 molecule, despite its established anti-tumor activity (Wang *et al.*, 2013; Kim *et al.*, 2018;  
78 Parrish *et al.*, 2018; Bayo *et al.*, 2018; Dalvi *et al.*, 2017).

79

80 We tested whether JIB-04 treatment could inhibit replication of a clinical isolate of SARS-  
81 CoV-2 (2019-nCoV/USA-WA1/2020 strain). Viral antigen staining showed that a 1-hour  
82 pre-treatment with JIB-04 suppressed SARS-CoV-2 infection in Vero E6 cells with an  
83 EC<sub>50</sub> value of 695 nM (95% confidence interval of 567-822 nM) (**Fig. 1B**). Cell viability did  
84 not fall below 50% even at 1 mM of JIB-04 treatment, making the selectivity index of JIB-  
85 04 higher than 1,000. Intracellular SARS-CoV-2 RNA levels also were reduced  
86 significantly by JIB-04, but not by camostat, a TMPRSS serine protease inhibitor (**Fig.**  
87 **1C**).

88

89 To examine whether JIB-04 targets SARS-CoV-2 spike protein-mediated entry or other  
90 post-entry pathways (*e.g.*, translation, replication, or assembly) shared between SARS-  
91 CoV-2 and other viruses, we tested JIB-04 against vesicular stomatitis virus (VSV) that  
92 expresses eGFP as a marker of infection (Cherry *et al.*, 2005) and a replication-

93 competent chimeric VSV in which the native glycoprotein (G) was replaced by the spike  
94 of SARS-CoV-2 (VSV-eGFP-SARS-CoV-2) (Case *et al.*, 2020). JIB-04 suppressed  
95 replication of both viruses in MA104 and Vero E6-TMPRSS2 cells (**Fig. 2A-B**). Flow  
96 cytometry analysis of cells at 6h post-infection revealed a reduction in eGFP expression  
97 demonstrating that the inhibitory effect of JIB-04 occurs during either entry or gene-  
98 expression (**Fig. 2B**). Virus-infected cells also showed less GFP intensity with JIB-04  
99 treatment (**Fig. S2A**). JIB-04 inhibited VSV-SARS-CoV-2 infection dose-dependently  
100 without apparent cytotoxicity (**Fig. 2C** and **S2B**), which became more apparent when cells  
101 were inoculated with virus at a low multiplicity of infection (MOI) (**Fig. S2C**). At 30  $\mu$ M,  
102 JIB-04 treatment resulted in a 100-fold reduction of intracellular VSV-SARS-CoV-2 RNA  
103 levels (**Fig. S2D**).

104

105 We next evaluated the antiviral activity of JIB-04 against other viruses. Though JIB-04 did  
106 not diminish replication of herpes simplex virus 1, it inhibited the replication of vaccinia  
107 virus, another DNA virus, and several strains of rotavirus (RV), a double-stranded RNA  
108 virus (RV) (**Fig. 2C-D**). JIB-04 also inhibited the replication of transmissible gastroenteritis  
109 virus (TGEV) (**Fig. 2D-E** and **Fig. S2E**), a porcine coronavirus that infects the small  
110 intestine of pigs and causes lethal diarrhea (Saif, 2004). This indicates that the antiviral  
111 effect of JIB-04 is not limited to single-stranded RNA viruses in cell culture.

112

113 Although JIB-04 inhibits the replication of both SARS-CoV-2 and VSV-SARS-CoV-2 in  
114 monkey kidney epithelial cell lines, a primary *in vivo* target of SARS-CoV-2 is ciliated  
115 airway epithelial cells (Hou *et al.*, 2020). We therefore examined the inhibitory effect if

116 JIB-04 on SARS-CoV-2 infection of the human lung epithelial cell line Calu-3 (Hoffmann  
117 *et al.*, 2020; Sheahan *et al.*, 2020). We validated that JIB-04 retained its antiviral activity  
118 against VSV-SARS-CoV-2 in Calu-3 cells (**Fig. 2G**). VSV-SARS-CoV-2 replication was  
119 also inhibited by JIB-04 in HEK293 cells ectopically expressing human ACE2, an entry  
120 receptor for SARS-CoV-2 (Hoffmann *et al.*, 2020), with or without ectopic TMPRSS2  
121 expression (**Fig. 2G**).

122  
123 We next sought to understand the mechanisms of antiviral activity of JIB-04. Although  
124 JIB-04 has been previously connected to interferon (IFN) and autophagy activation (Wang  
125 *et al.*, 2013; Xu *et al.*, 2018), the antiviral activity that we observed was independent of  
126 these pathways. JIB-04 treatment did not lead to the induction of IFN and IFN-stimulated  
127 gene expression or the formation of LC3-positive punctate structures (**Fig. S3A-B**). To  
128 explore the mechanisms of antiviral action, we utilized a drug combination approach.  
129 When a combination of JIB-04 with chloroquine was evaluated based on the highest  
130 single agent (HAS) synergy model with SynergyFinder 2.0 (Ianevski *et al.*, 2020), JIB-04  
131 was shown to exert a synergistic antiviral effect with chloroquine in MA104 cells (**Fig. 3A**).  
132 A combination of JIB-04 and camostat also was synergistically antiviral in Calu-3 cells  
133 (**Fig. S3C**), indicating that JIB-04 likely targets a different pathway.

134  
135 A possible antiviral role for JIB-04 at a post-entry step was supported by the time of  
136 addition experiments (**Fig. 3B**). A 1-h pre-treatment of cells with JIB-04 reduced SARS-  
137 CoV-2 spike mRNA transcription following VSV-SARS-CoV-2 infection (**Fig. 3C**), and  
138 translation of newly synthesized spike protein, which could not be achieved with

139 Actinomycin D treatment (**Fig. 3D**). These results suggest that JIB-04 might repress virus  
140 replication by interfering with the viral RNA transcription or stability.

141

142 We also assessed whether the antiviral activity of JIB-04 is linked to its epigenetic  
143 modulatory action. Unlike its E-isomer, the Z-isomer of JIB-04 does not inhibit histone  
144 demethylases at similar doses (Wang *et al.*, 2013). When we compared the antiviral  
145 efficacy of these two JIB-04 isomers against VSV-SARS-CoV-2 in MA104 cells, the Z-  
146 isomer did not inhibit the replication of virus (**Fig. 3E**). The disparity between the isomers  
147 suggests that epigenetic enzyme inhibition is involved in antiviral mechanisms of JIB-04.

148 To examine the cellular pathways modulated by JIB-04, we performed small interfering  
149 RNA (siRNA)-mediated knockdown of JIB-04 cellular targets (*i.e.*, histone demethylases  
150 KDM4B, KDM4C, KDM5A, or KDM5B (Wang *et al.*, 2013)). Knockdown of each gene  
151 successfully recapitulated the antiviral effect of JIB-04 (**Fig. 3F** and **Fig. S3E**). These  
152 results led us to hypothesize that JIB-04 treatment promoted H3K9 and H3K27  
153 methylation and silenced expression of a subset of genes, triggering the antiviral effect.

154 To identify potential target genes, we performed RNA-sequencing on the cells pre-treated  
155 with vehicle or JIB-04 with or without virus infection (**Fig. 3G**). Pathway analysis revealed  
156 dampened metabolic signaling pathways such as cytochrome P450 system in JIB-04  
157 treated cells (**Fig. S3F**). Specifically, JIB-04 treatment downregulated two cytochrome  
158 P450 enzymes, *CYP1A1* and *CYP1B1*, and aryl hydrocarbon receptor repressor (*AHRR*),  
159 which represses transactivator of *CYP1A1* and *CYP1B1* (Karchner *et al.*, 2002). We  
160 validated by quantitative PCR that JIB-04 treatment reduced *CYP1A1*, *CYP1B1*, and  
161 *AHRR* mRNA levels by 4-6-fold (**Fig. 3H**). To explore the pharmacological utility of this

162 finding, we tested the antiviral activity of cytochrome P450 enzyme inhibitors fluoxetine  
163 and fluvoxamine (Hemeryck and Belpaire, 2002). Both compounds inhibited the  
164 replication of VSV-SARS-CoV-2 (**Fig. 3I**) and wild-type SARS-CoV-2 (**Fig. 3J**).

165  
166 Given that JIB-04 prevents coronavirus replication *in vitro*, we used a neonatal pig TGEV  
167 infection model (Luo *et al.*, 2019) to assess the efficacy of JIB-04 against coronavirus  
168 infection *in vivo*. Two-day old piglets were injected via an intraperitoneal route with JIB-  
169 04 twice before the oral inoculation of TGEV (**Fig. 4A**). We monitored body weight on a  
170 daily basis and recorded diarrhea development and mortality every 6 h. The animals in  
171 the control group lost more weight and had more severe diarrhea than those receiving  
172 JIB-04 (**Fig. S4A-B**). At 2 days post infection, 3 of 5 piglets in the DMSO group  
173 succumbed to infection as compared to 1 out of 5 animals in the JIB-04 group (**Fig. 4B**).  
174 Consistent with our *in vitro* results (**Fig. 2E-F**), the TGEV viral burden throughout the  
175 gastrointestinal tract was substantially lower in the JIB-04 treated group (**Fig. 4C-D**). JIB-  
176 treated animals also had lower number of viral antigen positive cells in their intestinal  
177 epithelium (**Fig. S4C**) and showed less enteropathy than the control group (**Fig. 4E**).  
178 Taken together, our data demonstrate *in vivo* antiviral activity of JIB-04 against a porcine  
179 coronavirus.

180

## 181 **DISCUSSION**

182

183 Using a repurposed compound screening approach, we identified drugs with reported  
184 inhibitory activity against SARS-CoV-2, such as tetrandrine (Ou *et al.*, 2020) and arbidol



185 (Wang *et al.*, 2020b). We also characterized a number of small-molecules (JIB-04, AG-  
186 1478, nigericin, etc.) without known antiviral activity as inhibitors of SARS-CoV-2 infection.  
187 While this manuscript was in preparation, a new study identified thapsigargin, the  
188 compound that showed the highest anti-SARS-CoV-2 activity in our screen as a broad  
189 antiviral against coronavirus (Al-Beltagi *et al.*, 2021), which validates our screen approach.  
190 Notably, several top hit compounds in the screen converge on the endosomal trafficking  
191 pathway: brefeldin A, concanamycin A, tetrandrine, and U18666A. Furthermore, FTY720  
192 induced formation of enlarged endosome/lysosome structure, similar to that triggered by  
193 apilimod treatment (Kang *et al.*, 2020). All of these point to an important role of endosomal  
194 trafficking in SARS-CoV-2 entry and infection, at least in cell culture.

195

196 Our results highlight JIB-04 as a potential therapeutic for SARS-CoV-2 and suggest  
197 further evaluation of this drug that has mainly been associated with its anti-cancer  
198 activities. Another compound in our screen, GSK-J4, also is a histone demethylase  
199 inhibitor that targets KDM6B. However, unlike JIB-04, GSK-J4 failed to reduce viral  
200 burden in Vero E6 cells upon SARS-CoV-2 infection to an extent comparable to  
201 chloroquine. Thus, we speculate that there might be specific roles played by certain KDM  
202 family members in the interactions between the host and SARS-CoV-2.

203

## 204 **Limitations of the study**

205

206 We have tried to be careful about establishing the broad-spectrum antiviral activity of JIB-  
207 04. Indeed, we have shown examples from distinct virus families (double-strand DNA

208 virus: vaccinia virus; single-strand positive-strand RNA virus: SARS-CoV-2 and TGEV;  
209 single-strand negative-strand RNA virus: VSV and VSV-SARS-CoV-2; double-strand  
210 RNA virus: rotavirus). However, we have yet to test single-strand DNA viruses and  
211 retroviruses. We also did not examine whether JIB-04 has antiviral activity against the  
212 newly emerging SARS-CoV-2 variants. We showed that JIB-04 modulates cytochrome  
213 P450 genes and targeting these genes by well-established selective serotonin uptake  
214 inhibitor also led to the inhibition of SARS-CoV-2 replication. Nevertheless, we do not  
215 know how modulation of cytochrome P450 genes correlates with transcriptional  
216 repression of SARS-CoV-2 RNA that we observed after JIB-04 treatment. It is plausible  
217 that JIB-04 induces these two effects separately, which needs to be characterized in  
218 future studies. Lastly, though we provided evidence that JIB-04 protects against  
219 coronavirus infection *in vivo* using a porcine TGEV model, TGEV is an animal coronavirus  
220 that targets the enteric rather than the respiratory system. Protection against SARS-CoV-  
221 2 *in vivo* should be tested in a transgenic mouse or hamster model. Finally, while the  
222 distinct efficacy of the E vs Z isomers points to inhibition of Jumonji demethylases as  
223 contributing to the antiviral effects, direct evidence of this mechanism in multiple models  
224 would strengthen this conclusion.

225

## 226 **MATERIALS AND METHODS**

### 227 **Reagents, cells, and viruses**

228 **Reagents:** JIB-04 E-isomer used in *in vitro* assays (S7281, Selleckchem, 99.8% purity),  
229 JIB-04 E-isomer used in *in vivo* experiments (HY-13953, Med-ChemExpress),  
230 Actinomycin D (A5156, Sigma), Fluvoxamine maleate (S1336, Selleckchem), Fluoxetine

231 HCl (S1333, Selleckchem), low molecular weight poly(I:C) complexed with LyoVec (trl-  
232 picwlv, InvivoGen). EGFP-LC3 plasmid was a gift from Christina Stallings at Washington  
233 University School of Medicine. pUC19 empty plasmid was used as mock in all transfection  
234 experiments. JIB-04 Z-isomer used in control experiments by synthesized as originally  
235 described (Wang et al, 2013).

236

237 **Cells:** Vero E6 cells (CRL-1586, ATCC) and Vero cells (CCL81, ATCC) were cultured in  
238 DMEM supplemented with 10% fetal bovine serum (FBS), 10 mM HEPES, 1 mM sodium  
239 pyruvate, 0.1 mM non-essential amino acids, and 1X Penicillin-Streptomycin-Glutamine.  
240 Calu-3 cells (HTB-55, ATCC) and swine ST cells (CRL-1746, ATCC) were DMEM  
241 supplemented with 10% FBS and 1 X Penicillin-Streptomycin-Glutamine. HEK293,  
242 HEK293-hACE2, and HEK293-hACE2-TMPRSS2 cells were cultured in complete DMEM  
243 containing G418 and/or blasticidin and used as previously described (Zang *et al.*, 2020a).  
244 MA104 and Vero E6-TMPRSS2 cells were cultured as before (Zang *et al.*, 2020b).

245

246 **Viruses:** Rhesus RV RRV strain, bovine RV UK strain, and porcine RV NJ2012 strain  
247 (Genbank: MT874983-MT874993) were propagated and titrated as before (Ding *et al.*,  
248 2018). Vaccinia virus MVA strain was used as before (Li *et al.*, 2017). HSV-1 syn17+  
249 strain was a gift from Ann Arvin at Stanford University. TGEV JS2012 strain was  
250 propagated as before (Guo *et al.*, 2020). TGEV was titrated by serial dilutions in cells in  
251 96-well plates that were seeded at a density of  $1 \times 10^4$  cells per well. Cytopathic effects  
252 were observed at 3-7 dpi and the TCID<sub>50</sub> values were calculated and converted to PFU/ml.  
253 A clinical isolate of SARS-CoV-2 (2019-nCoV/USA-WA1/2020 strain) was obtained from

254 the Centers for Disease Control and Prevention. A SARS-CoV-2 mNeonGreen reporter  
255 virus was used as previously reported (Xie *et al.*, 2020). Both the clinical isolate and the  
256 mNeonGreen SARS-CoV-2 viruses were propagated in Vero CCL81 cells and titrated by  
257 focus-forming assays on Vero E6 cells. Recombinant VSV-eGFP (Cherry *et al.*, 2005)  
258 and VSV-eGFP-SARS-CoV-2 were previously described (Case *et al.*, 2020). Cells  
259 infected with viruses expressing GFP were imaged with an ECHO REVOLVE 4  
260 fluorescence microscope. Plaque assays were performed in MA104 cells seeded in 6-  
261 well plates using an adapted version of the rotavirus plaque assay protocol (Ding *et al.*,  
262 2018).

263

#### 264 **Inhibitor screen**

265 The small-molecule inhibitors used in this study are from in-house collection and the  
266 COVID Box (Medicines for Malaria Venture; [www.mmv.org/mmv-open/covid-box](http://www.mmv.org/mmv-open/covid-box)).  
267 Compound names, vendors, and catalog numbers are listed in **Table S1**. At 24 hpi, cells  
268 were fixed in 4% paraformaldehyde (PFA) in PBS and stained with Hoechst 33342. The  
269 levels of viral antigens, reflected by mNeonGreen signals, were scanned by Amersham  
270 Typhoon 5 (GE). Image background was subtracted using rolling ball algorithm (radius =  
271 5 pixels). To minimize imaging artifacts and well-to-well variation, we removed the region  
272 which fell below the threshold calculated by Moments algorithm. The number of positive  
273 pixels and total intensity (after background subtraction) were computed for each well and  
274 log<sub>10</sub> transformed. The number of cells in each well was quantified based on Hoechst  
275 33342 staining detected by Cytation 3 imaging reader (BioTek). Image analysis was

276 performed using ImageJ and customized R scripts. The quantification of mNeonGreen  
277 and Hoechst 33342 is provided in **Dataset S1**.

278

### 279 **Cell cytotoxicity assay**

280 The viability of Vero E6 and MA104 cells after drug treatment was determined using the  
281 Cell Counting Kit 8 (ab228554, Abcam). Briefly, cells in 96-well plates were treated with  
282 JIB-04 at desired concentrations at 37°C. After a 25-h incubation, the inhibitor-containing  
283 medium was replaced with fresh complete medium with 10 µl of WST-8 solution in each  
284 well. The cells were incubated at 37 °C for 2 h with protection from light. Absorbance at  
285 460nm was measured using Gen5 software and a BioTek ELx800 Microplate Reader.

286

### 287 **RNA extraction and quantitative PCR**

288 Total RNA was extracted from cells using RNeasy Mini kit (Qiagen). For spike plasmid  
289 transfection experiments, total RNA was extracted using Aurum Total RNA Mini Kit  
290 (Biorad) with DNase digestion. Complementary DNA was synthesized with High Capacity  
291 cDNA Reverse Transcription kit (Thermo Fisher) as previously described (Bolen *et al.*,  
292 2013). Quantitative PCR was performed using AriaMX (Agilent) with 12.5 µl of either  
293 Power SYBR Green master mix or Taqman master mix (Applied Biosystems) in a 25 µl  
294 reaction. Gene expression was normalized to the housekeeping gene GAPDH. All SYBR  
295 Green primers and Taqman probes used in this study are listed in **Table S2**.

296

### 297 **Western blotting**

298 Cells were lysed in RIPA buffer supplemented with protease inhibitor cocktail and  
299 phosphatase inhibitor. Lysates were boiled for 5 min in 1 x Laemmli Sample Buffer (Bio-  
300 Rad) containing 5%  $\beta$ -mercaptoethanol. Proteins were resolved in SDS-PAGE and  
301 detected as described (Ding *et al.*, 2014) using the following antibodies: GAPDH (631402,  
302 Biologend), rotavirus VP6 (rabbit polyclonal, ABclonal technology), and SARS-CoV-2 S2  
303 (40592-T62, Sino Biological). Secondary antibodies were anti-rabbit (7074, Cell Signaling)  
304 or anti-mouse (7076, Cell Signaling) immunoglobulin G horseradish peroxidase-linked  
305 antibodies. Protein bands were visualized with Clarity ECL Substrate (Bio-rad) and a  
306 Biorad Gel Doc XR system.

307

#### 308 **Small interfering RNA transfection**

309 HEK293 cells were transfected using Lipofectamine RNAiMAX Transfection Reagent  
310 (Thermo Fisher). Cells were harvested at 48 h post transfection, and knockdown  
311 efficiency was determined by RT-qPCR. siRNA transfected cells were infected with PoRV  
312 (MOI=0.01) for 12 h and viral RNA copy numbers were examined by RT-qPCR. All siRNA  
313 used in this study were designed and synthesized by GenePharma (Shanghai, China)  
314 and their sequences of siRNAs are listed in **Table S2**.

315

#### 316 **Flow cytometry**

317 Vero E6-TMPRSS2 cells were inoculated with VSV-GFP or VSV-SARS-CoV-2 at an MOI  
318 of 3 for 1 h at 37°C. At 6 hpi, cells were harvested and fixed in 4% PFA in PBS. Percentage  
319 of GFP positive cells and GFP intensity were determined by BD LSRFortessa™ X-20 cell  
320 analyzer and analyzed by FlowJo v10.6.2 (BD).

321

## 322 **RNA-sequencing**

323 HEK293 cells were pre-treated with JIB-04 (10  $\mu$ M) for 12 h, and mock or porcine RV-  
324 infected (MOI=0.01) for another 12 h. Total RNA from cells in triplicate was extracted  
325 using RNeasy Mini kit (Qiagen). RNA sample quality was measured by both NanoDrop  
326 spectrophotometer (Thermo Fisher) and Bioanalyzer 2100 (Agilent). Libraries were  
327 sequenced on the Illumina NovaSeq 6000 platform. Differential gene expression analysis  
328 was performed using DESeq2. The RNA-seq raw and processed datasets were deposited  
329 onto NCBI Gene Expression Omnibus database (GSE156219).

330

## 331 **TGEV piglet infection**

332 Newborn piglets (Landrace  $\times$  Yorkshire) were spontaneously delivered from sows, and  
333 their body weights were recorded at birth. Fifteen neonatal male pigs at birth were  
334 obtained from a TGEV-free farm in Nanjing without suckling. All piglets were confirmed  
335 negative for TGEV by RT-PCR and ELISA (IDEXX, USA). The pigs were randomly  
336 separated into three groups, housed in separate rooms, and fed the same artificial milk  
337 substitutes that meet the nutrient and energy recommendations of the National Research  
338 Council [NRC, 2012] at the animal facility of the Institute of Veterinary Medicine, Jiangsu  
339 Academy of Agricultural Sciences, Nanjing, Jiangsu Province. The experiments were  
340 divided into three groups: a DMSO inoculation control group (control, n=5); a DMSO  
341 inoculation and TGEV infection group (TGEV-DMSO, n=5); a JIB-04 inoculation and  
342 TGEV infection group (TGEV-JIB-04, n=5)). Neonatal pigs were intraperitoneally injected  
343 twice with JIB-04 (75 mg/kg) or DMSO at 24 h and 6 h prior to TGEV infection. TGEV-

344 DMSO and TGEV-JIB-04 groups were orally infected with  $1 \times 10^{7.25}$  ( $1.778 \times 10^7$ ) TCID<sub>50</sub>  
345 (equivalent to  $1.245 \times 10^7$  PFU) of TGEV in 1.5 ml of DMEM per pig. Neonatal pigs were  
346 weighed and observed for clinical signs every 8 h throughout the study. Serum samples  
347 were collected from each pig at 24 and 48 hpi to detect specific anti-TGEV antibodies.  
348 The occurrence of diarrhea was monitored, and its severity was recorded based on an  
349 established scoring system (Li *et al.*, 2017). In brief, diarrhea was scored on the basis of  
350 color, consistency, and amount, and numbered as follows: 0 = normal; 1 = pasty; 2 =  
351 semi-liquid; 3 = liquid, and score  $\geq 2$  considered as diarrhea. At 48 hpi, all pigs were  
352 euthanized, and intestinal tissues were collected for pathological examination and viral  
353 load analysis using RT-qPCR and primers in **Table S2**.

354

### 355 **Histopathological and immunofluorescence analysis**

356 Intestinal tissues harvested from pigs were fixed in 4% PFA in PBS and incubated in 50%  
357 ethanol overnight. After fixation, tissues were embedded in paraffin, sectioned, and  
358 subjected to hematoxylin and eosin staining by standard procedures. For  
359 immunofluorescence analysis, samples were incubated with rabbit anti-TGEV-N antibody  
360 (1:500, DA0224, Shanghai YouLong Biotech) for 30 min at 37 °C. After three washes,  
361 samples were stained with Cy3-conjugated goat anti-rabbit secondary antibody  
362 (Beyotime) and DAPI (Invitrogen). Images were obtained using a fluorescence  
363 microscope (Carl Zeiss).

364

### 365 **Ethics statement**



366 Animal experiments were approved by the Committee on the Ethics of Animal Care and  
367 Use of the Science and Technology Agency of Jiangsu Province. The approval ID is  
368 NKYVET 2014-63, granted by the Jiangsu Academy of Agricultural Sciences  
369 Experimental Animal Ethics Committee. All efforts were made to minimize animal  
370 suffering. The virus challenge and tissue collection were performed in strict accordance  
371 with the guidelines of Jiangsu Province Animal Regulations (Decree No. 2020-18).

372

### 373 **Statistical analysis**

374 All bar graphs were displayed as means  $\pm$  standard error of mean (SEM). Statistical  
375 significance in data Fig. 2E, 2F, 3C, 4C, and 4D was calculated by Student's *t* test using  
376 Prism 8.4.3 (GraphPad). Statistical significance in data Fig. 1C, 2D, 2G, 3B, 3E, 3G, S3A,  
377 S3C, and S4B was calculated by pairwise ANOVA using Prism 8.4.3. Non-linear  
378 regression (curve fit) was performed to calculate EC<sub>50</sub> and CC<sub>50</sub> values for Fig. 1B, 2A,  
379 and 2C using Prism 8.4.3. HSA synergy model was used to calculate the synergy scores  
380 of dose-response data in Fig. 3A. Gehan-Breslow-Wilcoxon test was used to compare  
381 the survival curves in Fig. 4B. All data were presented as asterisks (\* $p \leq 0.05$ ; \*\* $p \leq 0.01$ ;  
382 \*\*\* $p \leq 0.001$ ). All experiments other than Fig. 1A, 3I, and 4 were repeated at least twice.  
383 The raw data are included in **Table S3**.

384

### 385 **SUPPLEMENTARY MATERIALS**

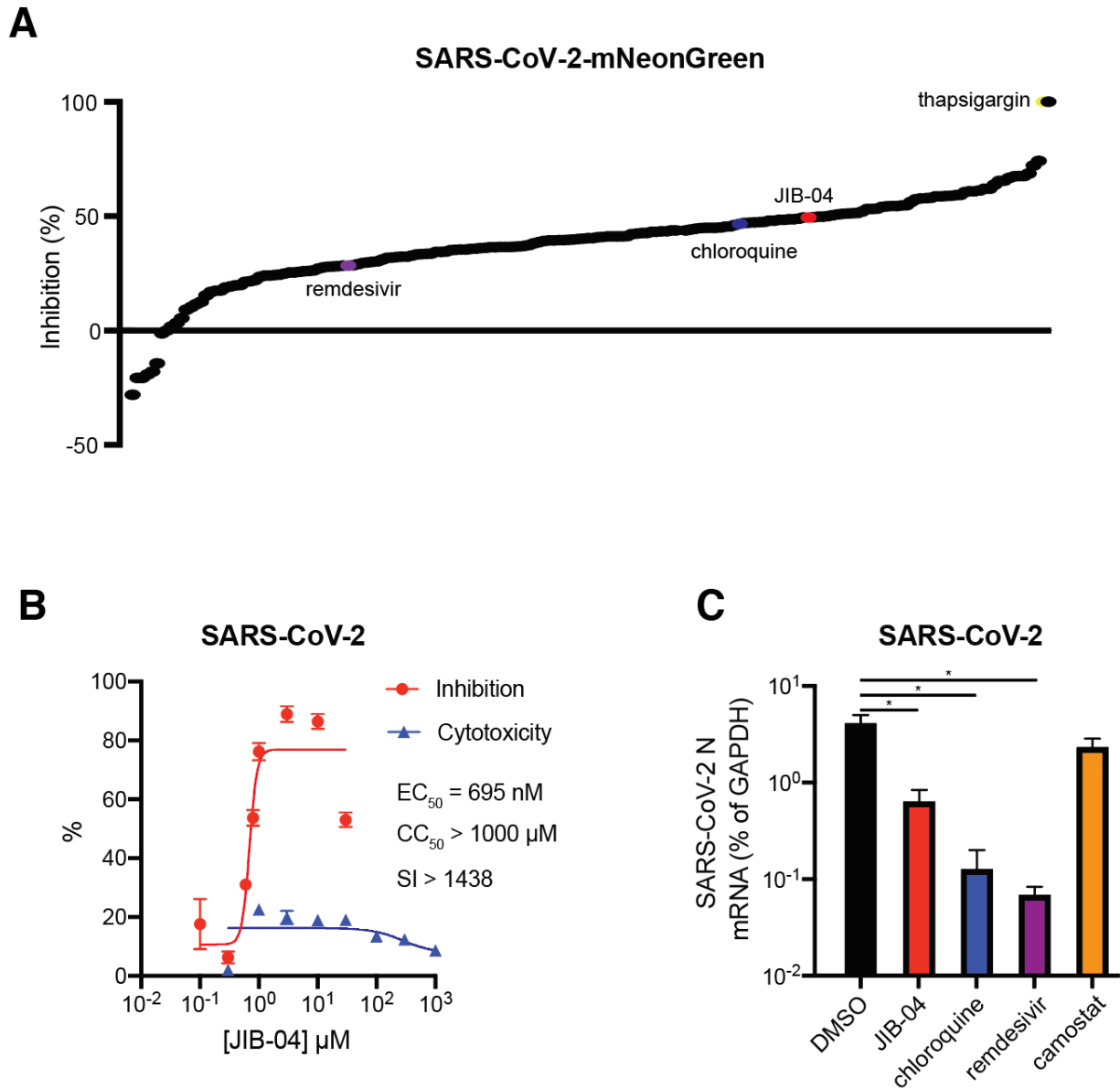
386 Table S1. List of chemicals used in the anti-SARS-CoV-2 compound screen

387 Table S2. List of qPCR primers and siRNA

388 Table S3. Raw data

389

390 **Figures and Legends**  
391



392  
393

394 **Fig. 1. JIB-04 inhibits SARS-CoV-2 replication**

395 (A) Small molecule inhibitor screen. Vero E6 cells were treated with individual  
396 compounds (listed in Table S1) at 10  $\mu$ M for 1 hour (h) and infected with SARS-  
397 CoV-2-mNeonGreen (MOI=0.5). At 24 h post infection (hpi), cells were fixed, and  
398 nuclei were stained by Hoechst 33342. The intensities of mNeonGreen and

399 Hoechst were quantified by the Typhoon biomolecular imager and the Cytation  
400 plate reader, respectively. The ratio of mNeonGreen and Hoechst is plotted as  
401 percentage of inhibition.

402 (B) Dose-response curve of wild-type SARS-CoV-2 replication with JIB-04 treatment.

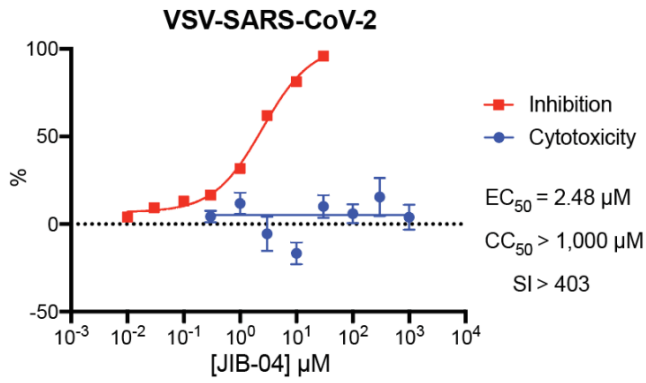
403 Vero E6 cells were treated with JIB-04 for 1 h and infected with a clinical isolate of  
404 SARS-CoV-2 (MOI=0.5). S protein levels were quantified at 24 hpi based on  
405 immunofluorescence. For CC<sub>50</sub> measurement, cells were treated with JIB-04 at 0.3  
406  $\mu$ M to 1 mM for 25 h. SI: selectivity index.

407 (C) Intracellular viral RNA levels of cells treated with compounds and subsequently  
408 infected with wild-type SARS-CoV-2. Vero E6 cells were treated with JIB-04 (10  
409  $\mu$ M), chloroquine (10  $\mu$ M), remdesivir (3  $\mu$ M), or camostat (10  $\mu$ M) for 1 h and  
410 infected with a clinical isolate of SARS-CoV-2 (MOI=0.5). SARS-CoV-2 RNA levels  
411 at 24 hpi were measured by RT-qPCR.

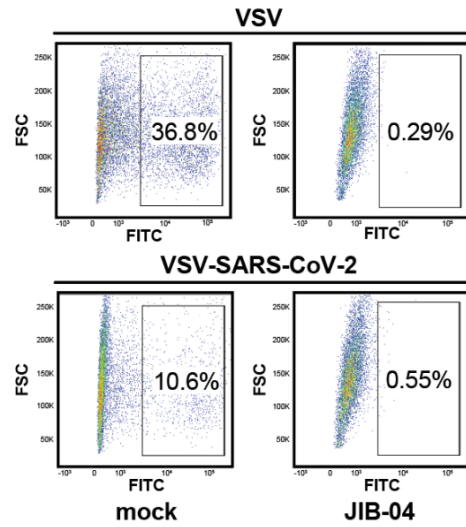
412 For all panels except A, experiments were repeated at least three times with similar  
413 results. Fig. 1A was performed once with raw data included in Dataset S1. Data  
414 are represented as mean  $\pm$  SEM. Statistical significance is from pooled data of the  
415 multiple independent experiments (\* $p \leq 0.05$ ).

416

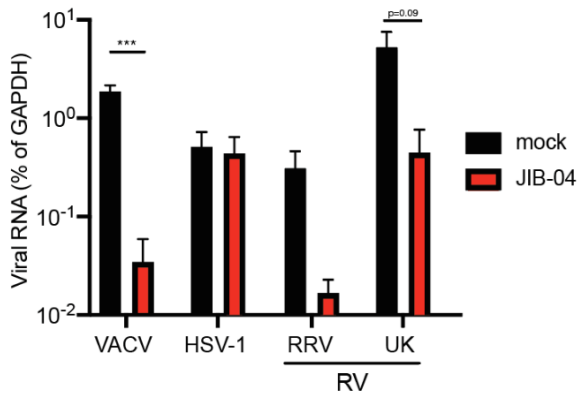
**A**



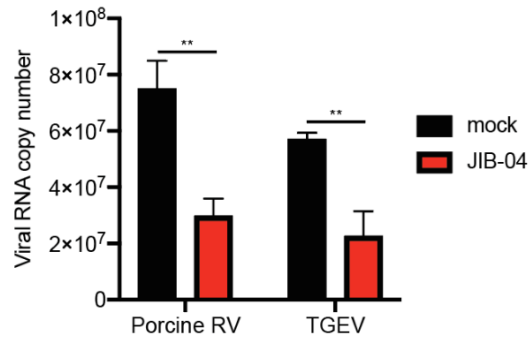
**B**



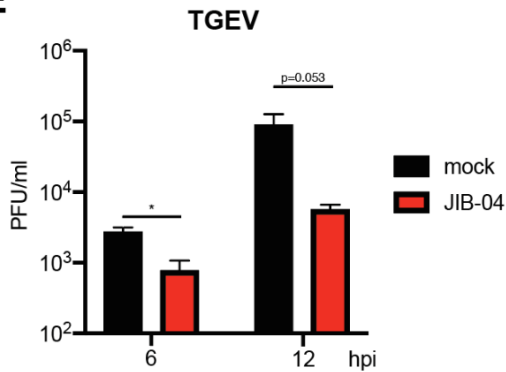
**C**



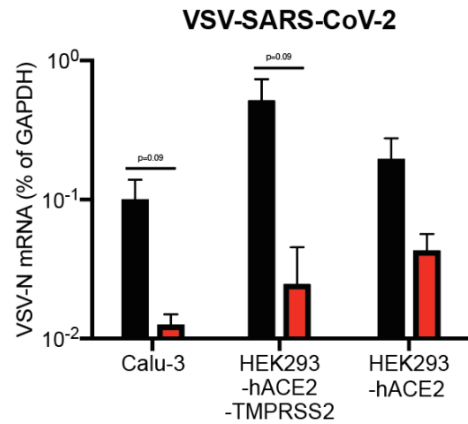
**D**



**E**



**F**



417  
418

419 **Fig. 2. JIB-04 broadly inhibits DNA and RNA viruses in different cell types**

420 (A) Dose-response analysis of VSV-SARS-CoV-2 replication and cytotoxicity with JIB-  
421 04 treatment. For EC<sub>50</sub> measurement, MA104 cells were treated with compounds  
422 at 0.01 to 30 µM for 1 h and infected with VSV-SARS-CoV-2 (MOI=3) for 24 h. For  
423 CC<sub>50</sub> measurement, cells were treated with compounds at 0.1 µM to 3 mM for 25  
424 h. SI: selectivity index.

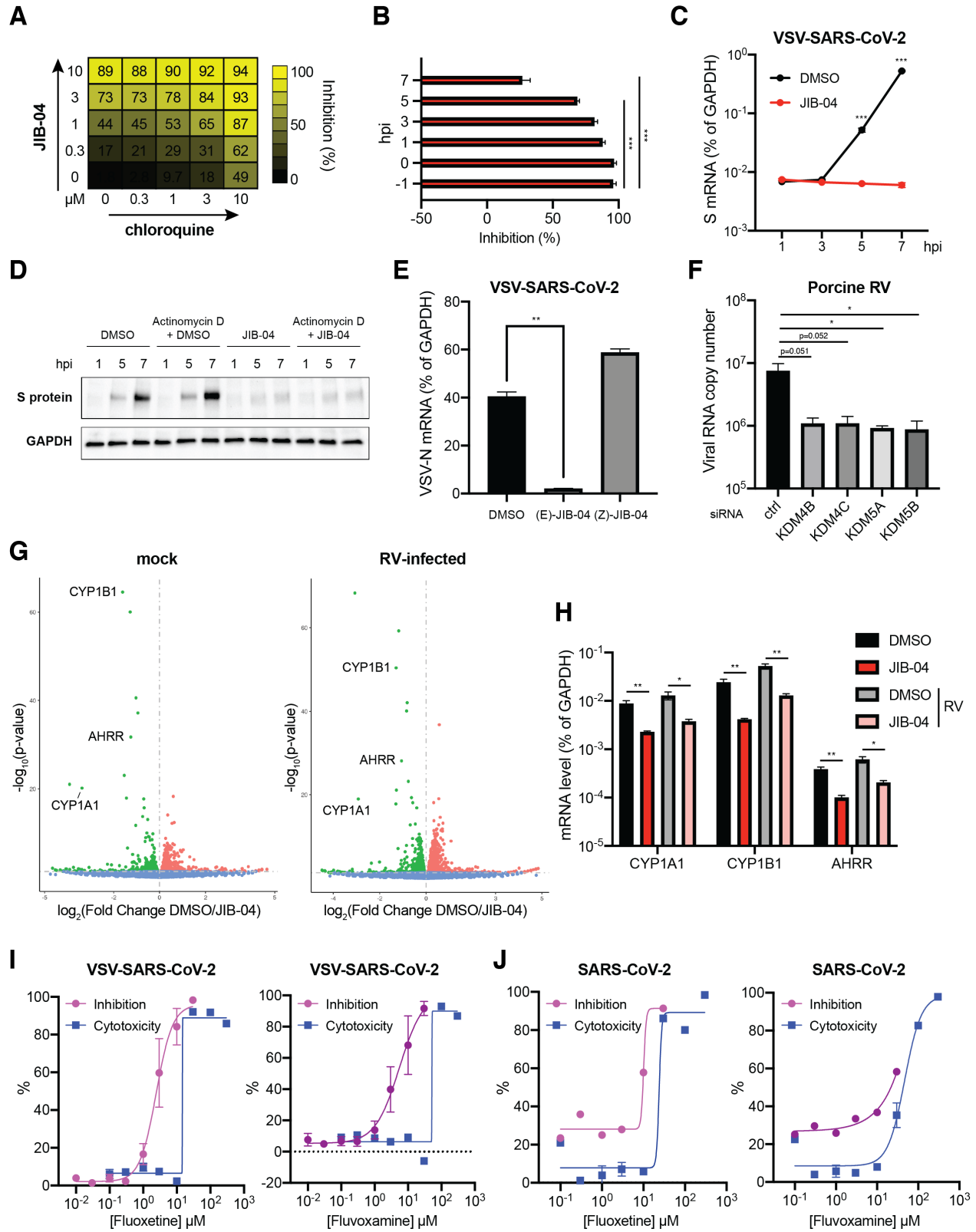
425 (B) Virus infectivity with JIB-04 treatment. Vero E6-TMPRSS2 cells were treated with  
426 compounds (10 µM) for 1 h and infected with VSV or VSV-SARS-CoV-2 (MOI=3).  
427 At 6 hpi, percentages of GFP positive cells were quantified by flow cytometry.

428 (C) Intracellular viral RNA levels with JIB-04 treatment. MA104 cells were treated with  
429 compounds (10 µM) for 1 h and infected with vaccinia virus (VACV), herpes  
430 simplex virus-1 (HSV-1), or rotavirus (RV, RRV and UK strains) (MOI=1). Viral  
431 RNA levels at 24 hpi were measured by RT-qPCR for VACV B10R, HSV-1 ICP-  
432 27, and RV NSP5, respectively.

433 (D) Viral RNA copy numbers with JIB-04 treatment. HEK293 cells were treated with  
434 JIB-04 (10 µM) for 6 h and infected with porcine rotavirus (MOI=0.01) for 6 h. ST  
435 cells were treated with JIB-04 (10 µM) for 12 h and infected with transmissible  
436 gastroenteritis virus (TGEV) (MOI=0.01) for 12 h. Viral RNA copy numbers were  
437 measured by RT-qPCR.

438 (E) TGEV titers in the cell supernatant with JIB-04 treatment. ST cells were treated  
439 with JIB-04 (10 µM) for 12 h and infected with TGEV (MOI=0.01). Virus titers at 6  
440 and 12 hpi were measured by plaque assays.

441 (F) Intracellular viral RNA levels with JIB-04 treatment in different cell types. Calu-3  
442 cells, HEK293-hACE2 and HEK293-hACE2-TMPRSS2 were treated with  
443 compounds (10  $\mu$ M) for 1 h and infected with VSV-SARS-CoV-2 (MOI=1). VSV  
444 RNA levels at 24 hpi were measured by RT-qPCR.  
445 All experiments were repeated at least three times with similar results. Data are  
446 represented as mean  $\pm$  SEM. Statistical significance is from pooled data of the  
447 multiple independent experiments (\* $p \leq 0.05$ ; \*\* $p \leq 0.01$ ; \*\*\* $p \leq 0.001$ ).  
448



449

450

451 **Fig. 3. JIB-04 exhibits distinct post-entry antiviral mechanisms**

452 (A) Drug combination dose-response matrix and VSV-SARS-CoV-2 replication.

453 MA104 cells were treated with JIB-04 and chloroquine for 1 h and infected with  
454 VSV-SARS-CoV-2 (MOI=3). GFP signals at 24 hpi were quantified to calculate the  
455 percentage of inhibition.

456 (B) Time of compound addition and VSV-SARS-CoV-2 replication. MA104 cells were  
457 treated with JIB-04 (10  $\mu$ M) at indicated time points relative to VSV-SARS-CoV-2  
458 infection (MOI=3, 0 hpi). GFP signals at 8 hpi were quantified to calculate the  
459 percentage of inhibition.

460 (C) Intracellular SARS-CoV-2 S RNA levels with JIB-04 treatment. MA104 cells were  
461 treated with JIB-04 (10  $\mu$ M) for 1 h and infected with VSV-SARS-CoV-2 (MOI=1)  
462 for 1, 3, 5, and 7 h. S RNA levels were measured by RT-qPCR.

463 (D) Western blot analysis of SARS-CoV-2 S protein levels with JIB-04 treatment.  
464 MA104 cells were treated with JIB-04 (10  $\mu$ M) for 1 h and infected with VSV-SARS-  
465 CoV-2 (MOI=1) for 1, 5, and 7 h. For Actinomycin D, 10  $\mu$ g/ml actinomycin D was  
466 added to the media 15 min before DMSO or JIB-04 treatment.

467 (E) Intracellular viral RNA levels of cells treated with JIB-04 E-isomer or Z-isomer and  
468 subsequently infected with VSV-SARS-CoV-2. MA104 cells were treated with JIB-  
469 04 isomer (10  $\mu$ M) for 1 h and infected with VSV-SARS-CoV-2 (MOI=1). VSV-N  
470 levels at 24 hpi were measured by RT-qPCR.

471 (F) Histone demethylase siRNA knockdown and RV replication. HEK293 cells were  
472 transfected with scrambled siRNA or siRNA targeting indicated histone



473 demethylases for 48 h and infected with porcine RV (MOI=0.01). Viral RNA copy  
474 numbers at 12 hpi were quantified by RT-qPCR.

475 (G) Volcano plot of differentially expressed transcripts with JIB-04 treatment and RV  
476 infection. HEK293 cells were treated with DMSO or JIB-04 (10  $\mu$ M) for 12 h, and  
477 mock-infected (left panel) or infected with porcine RV (MOI=0.01, right panel) for  
478 another 12 h. Red dots represent upregulated genes and green dots represent  
479 downregulated genes in JIB-04 treated cells.

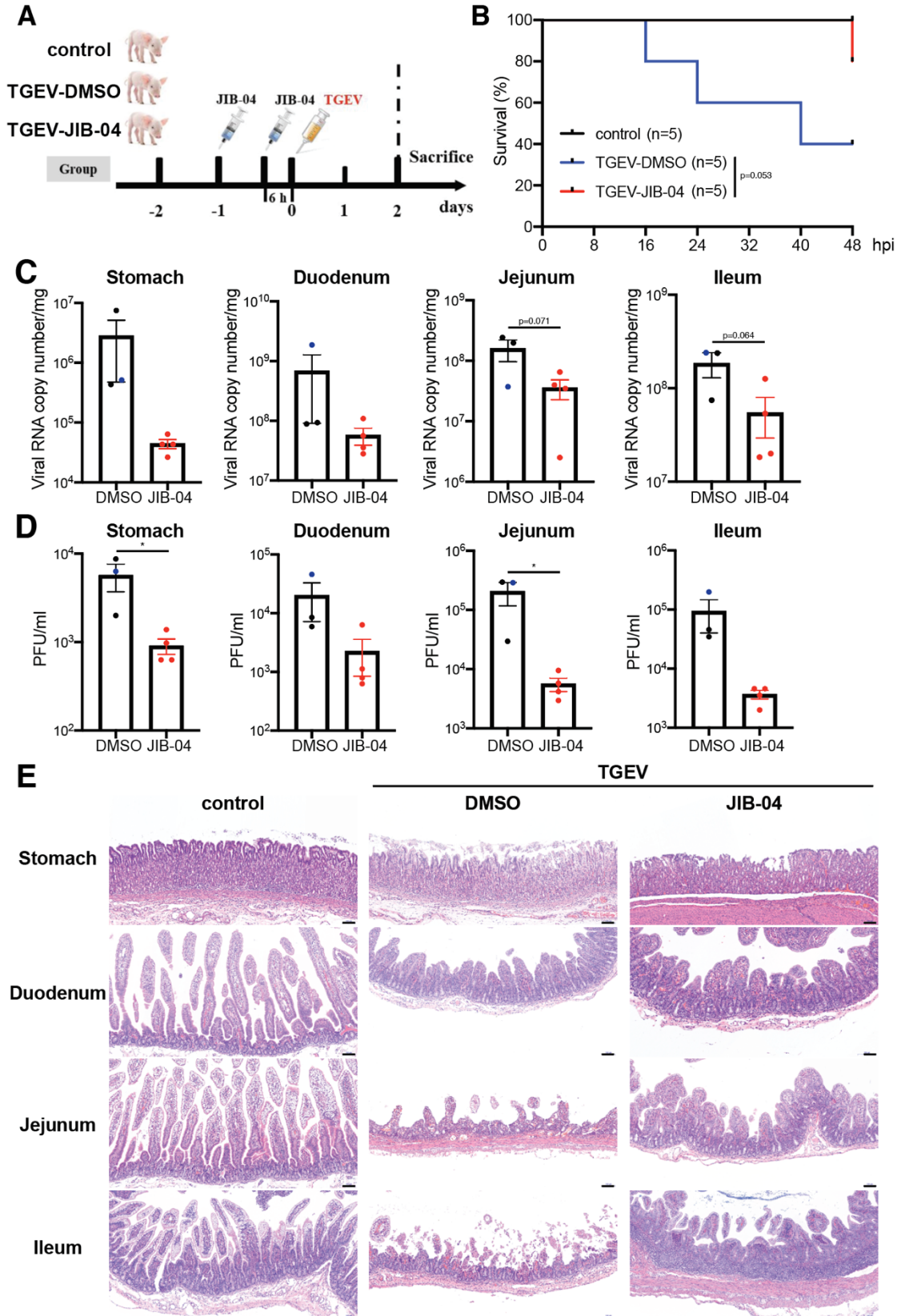
480 (H) Expression of three top genes in (G) with JIB-04 treatment. HEK293 cells were  
481 treated with JIB-04 (10  $\mu$ M) for 12 h and mock-infected or infected porcine RV  
482 (MOI=0.01) for 12 h. mRNA levels of *CYP1A1*, *CYP1B1*, and *AHRR* at 12 hpi were  
483 measured by RT-qPCR.

484 (I) Dose-response analysis of VSV-SARS-CoV-2 replication with fluoxetine or  
485 fluvoxamine treatment. MA104 cells were treated with compounds at 0.01 to 30  
486  $\mu$ M for 1 h and infected with VSV-SARS-CoV-2 (MOI=3). GFP signals at 24 hpi  
487 were quantified to calculate the percentage of inhibition. For  $CC_{50}$  measurement,  
488 cells were treated with compounds at 0.1  $\mu$ M to 300  $\mu$ M for 25 h.

489 (J) Dose-response analysis of wild-type SARS-CoV-2 replication with fluoxetine or  
490 fluvoxamine treatment. Vero E6 cells were treated with compounds for 1 h and  
491 infected with a clinical isolate of SARS-CoV-2 (MOI=0.5). S protein levels at 24 hpi  
492 were quantified based on immunofluorescence. For  $CC_{50}$  measurement, cells were  
493 treated with compounds at 0.1  $\mu$ M to 300  $\mu$ M for 25 h.

494 For all panels except A and J, experiments were repeated at least three times with  
495 similar results. Fig. 3A was performed twice. Inhibition assay in Fig. 3J was

496 performed once and cytotoxicity assay was performed in triplicates. Data are  
497 represented as mean  $\pm$  SEM. Statistical significance is from pooled data of the  
498 multiple independent experiments (\* $p \leq 0.05$ ; \*\* $p \leq 0.01$ ; \*\*\* $p \leq 0.001$ ).



499  
500

501 **Fig. 4. JIB-04 suppresses TGEV replication and pathogenesis in pigs**

502 (A) Experimental schemes for testing the protective efficacy of JIB-04 treatment  
503 against TGEV challenge in three groups of neonatal pigs. Control: DMSO injection,  
504 mock infection; TGEV-DMSO: DMSO injection, TGEV infection; TGEV-JIB-04:  
505 JIB-04 injection, TGEV infection.

506 (B) Survival curve of TGEV infected pigs with JIB-04 treatment. Neonatal pigs were  
507 intraperitoneally injected with vehicle control DMSO or JIB-04 and mock-infected  
508 or infected with  $1.2 \times 10^7$  PFU of TGEV. Survival was monitored every 8 h with  
509 data censored at 48 hpi, when all pigs were sacrificed.

510 (C) TGEV RNA copy numbers in the gastrointestinal (GI) tract of infected pigs. TGEV  
511 infected piglets were sacrificed at 48 hpi. For the DMSO group, two animals  
512 sacrificed at 48 hpi and one that died at 40 hpi (colored in blue) were examined.  
513 For the JIB-04 groups, four animals sacrificed at 48 hpi were examined. TGEV  
514 genome copy numbers at 48 hpi were quantified by RT-qPCR.

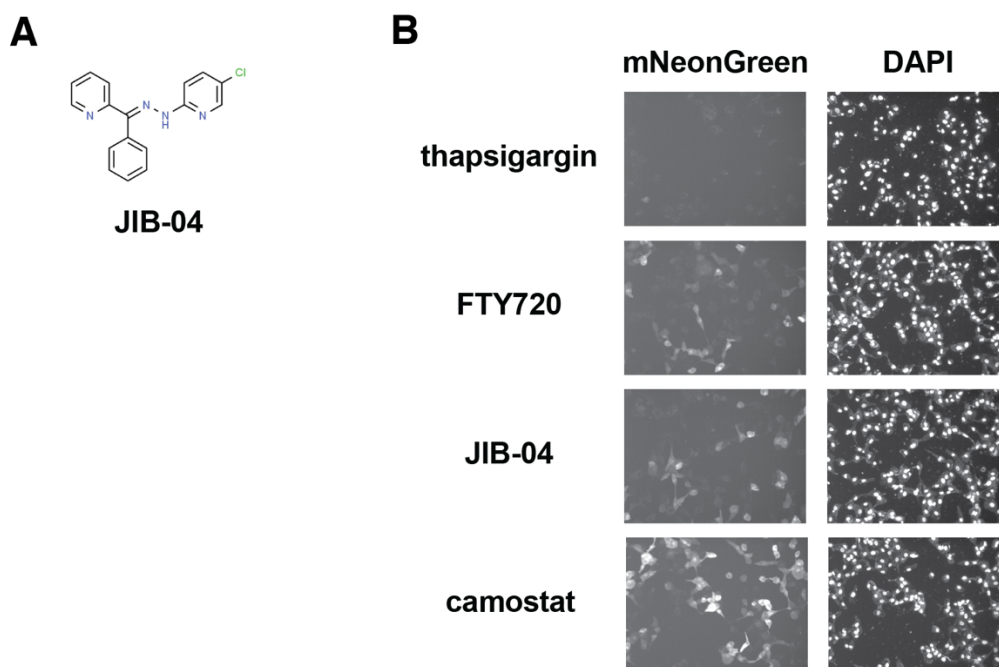
515 (D) Same as (C) except that virus titers were measured by plaque assays.

516 (E) Hematoxylin and eosin staining of different GI tract sections from pigs sacrificed at  
517 48 hpi. Representative images of 3 animals. Scale bar, 100  $\mu$ m.

518 Data are represented as mean  $\pm$  SEM. Statistical significance is from pooled data  
519 of the multiple independent experiments (\* $p \leq 0.05$ ).

520

521 **Supplemental Figures and Legends**



522

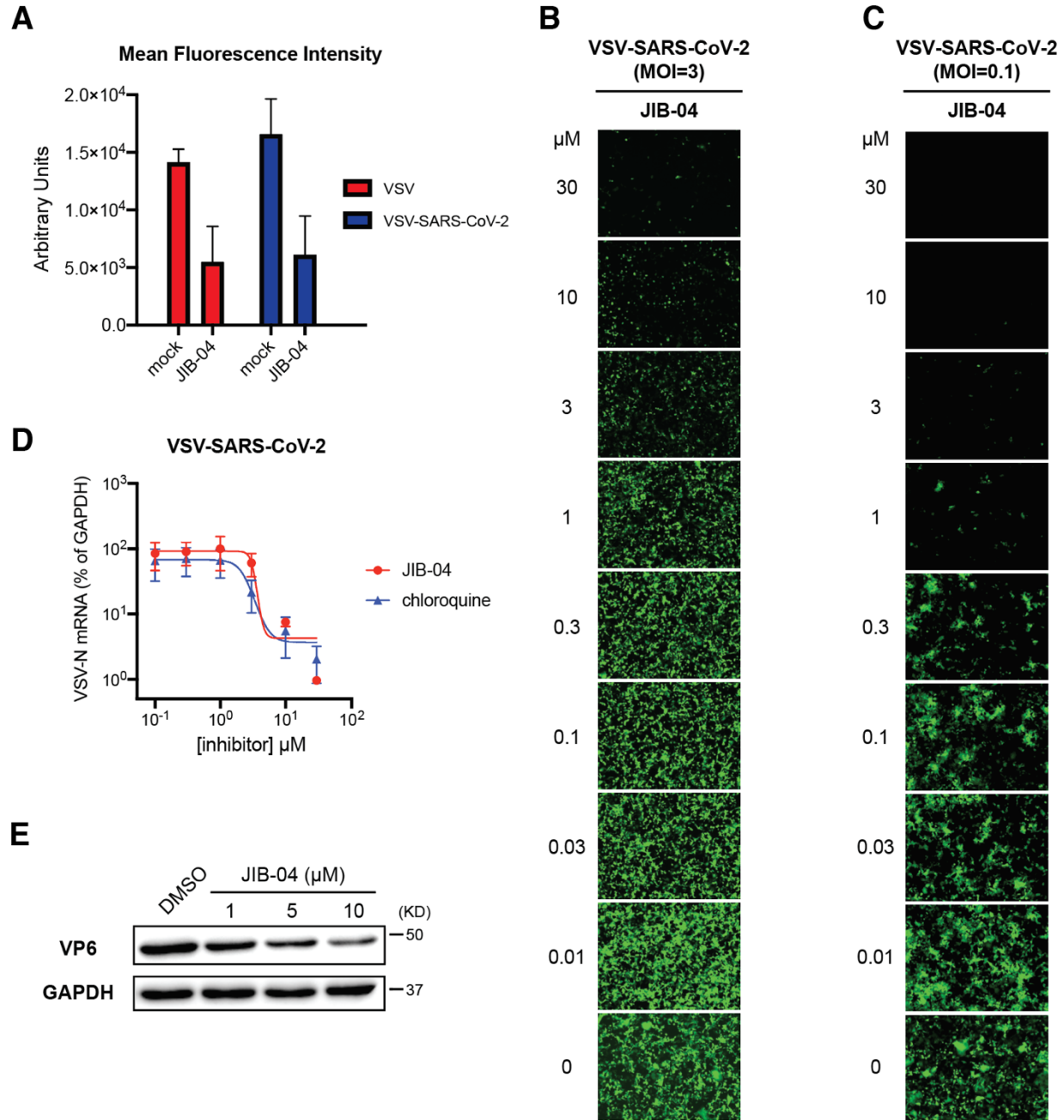
523

524 **Fig. S1. JIB-04 inhibits SARS-CoV-2 replication**

525 (A) Chemical structures of JIB-04 E-isomer from ChemSpider database.

526 (B) Representative images of Vero E6 cells infected by SARS-CoV-2-mNeonGreen

527 (MOI=0.5) at 24 hpi in Fig. 1A.



528

529 **Fig. S2. JIB-04 inhibits the replication of multiple viruses**

530 (A) Mean fluorescence intensity of GFP positive cells in Fig. 2B was quantified by flow  
531 cytometry.

532 (B) Dose-response analysis of VSV-SARS-CoV-2 replication with JIB-04 treatment.

533 MA104 cells were treated with JIB-04 at indicated concentrations for 1 h and

534 infected with VSV-SARS-CoV-2 (MOI=3). At 24 hpi, images of GFP positive  
535 infected cells were acquired by the ECHO fluorescence microscope.

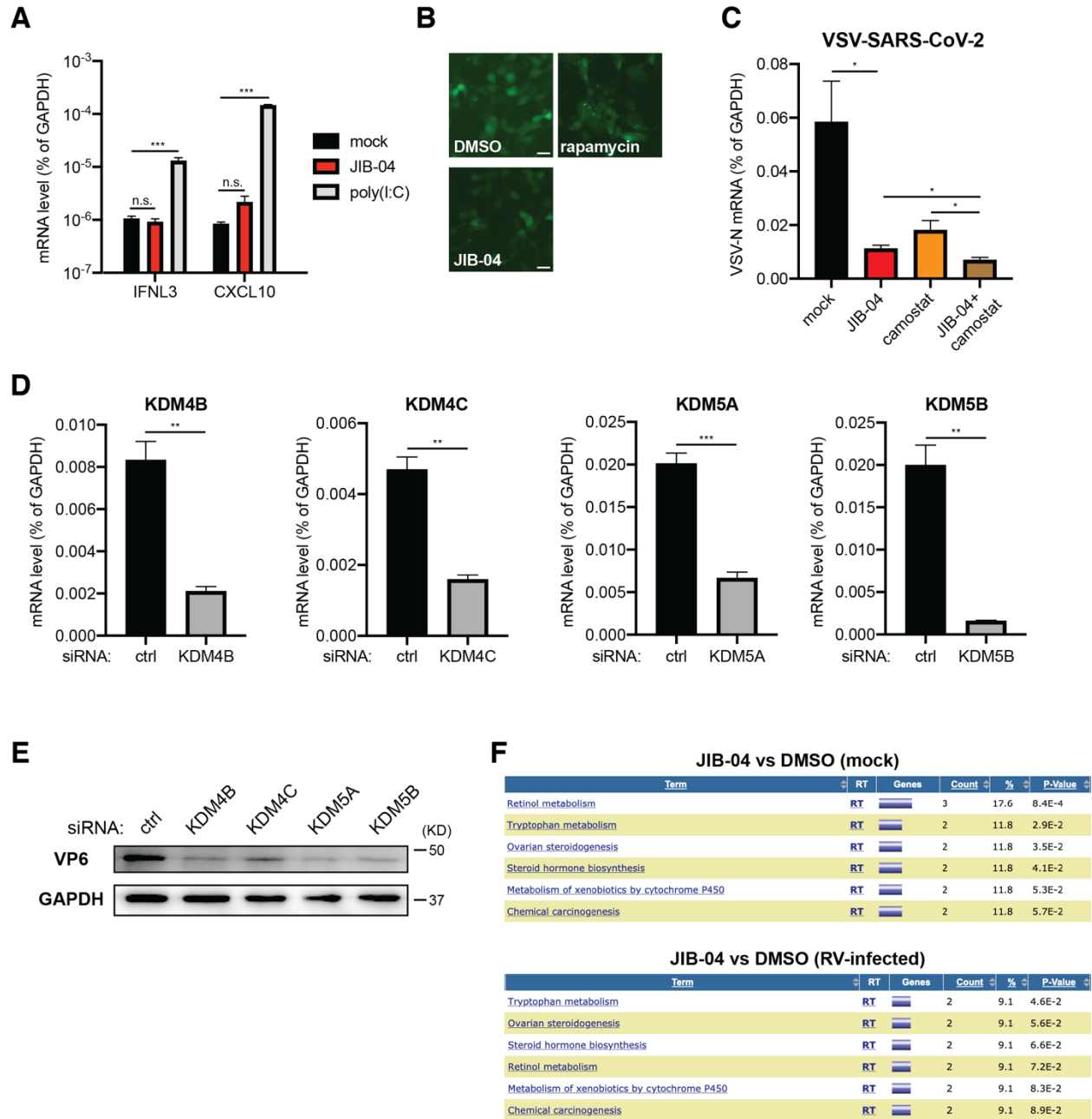
536 (C) Same as (B) except that cells were infected with an MOI of 0.1.

537 (D) Dose-response analysis of intracellular viral RNA levels with JIB-04 or chloroquine  
538 treatment. MA104 cells were treated with compounds at 0.1 to 30  $\mu$ M for 1 h and  
539 infected with VSV-SARS-CoV-2 (MOI=3). VSV RNA levels at 24 hpi were  
540 measured by RT-qPCR.

541 (E) Western blot analysis of RV antigen VP6 levels with JIB-04 treatment. HEK293  
542 cells were treated with JIB-04 at 1, 5, or 10  $\mu$ M for 6 h and infected with porcine  
543 RV (MOI=0.01) for 12 h. GAPDH was used as a loading control.

544 All experiments were repeated at least three times with similar results. Data are  
545 represented as mean  $\pm$  SEM.





546  
547

548 **Fig. S3. Inhibition or knockdown of specific KDM histone demethylases inhibits**

549 **virus replication**

550 (A) Expression of IFN and IFN-stimulated genes with JIB-04 treatment. HEK293 cells

551 were treated with JIB-04 (3  $\mu$ M) or transfected with low-molecular-weight poly(I:C)



552 (100 ng/ml) for 24 h. mRNA levels of IFNL3 and CXCL10 were measured by RT-  
553 qPCR.

554 (B) Autophagy formation with compound treatment. HEK293 cells were transfected  
555 with EGFP-LC3 plasmid for 24 h and treated with rapamycin (100 nM) or JIB-04 (3  
556  $\mu$ M) for another 18 h. GFP positive punctate structures indicate autophagy  
557 activation. Scale bar, 20  $\mu$ m.

558 (C) Intracellular viral RNA levels with JIB-04 and camostat treatment. Calu-3 cells were  
559 treated with compounds (10  $\mu$ M) for 1 h and infected with VSV-SARS-CoV-2  
560 (MOI=3). VSV RNA levels at 24 hpi were measured by RT-qPCR.

561 (D) siRNA-mediated knockdown of JIB-04 target histone demethylases. HEK293 cells  
562 were transfected with scrambled siRNA or siRNA targeting indicated histone  
563 demethylases for 48 h. mRNA levels of indicated histone demethylases were  
564 measured by RT-qPCR.

565 (E) Western blot analysis of RV antigen VP6 levels in cells with histone demethylase  
566 siRNA knockdown. HEK293 cells were transfected with scrambled siRNA or siRNA  
567 targeting indicated histone demethylases for 48 h and infected with porcine RV  
568 (MOI=0.01) for 12 h.

569 (F) Pathway enrichment analysis of gene expression regulated by JIB-04 treatment.  
570 Downregulated genes in Fig. 3F with p values < 1e-10 were analyzed by DAVID  
571 functional annotation.

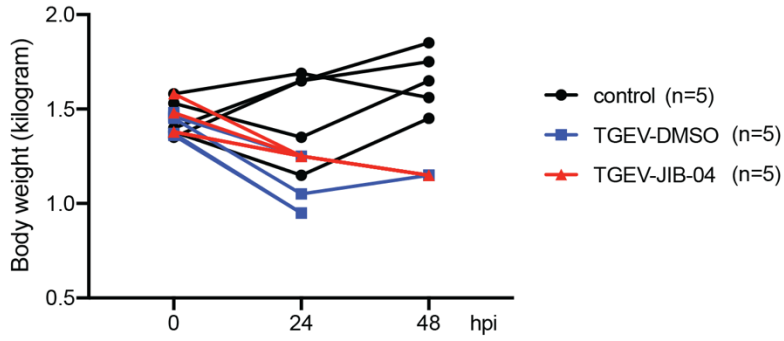
572 For all panels except B, experiments were repeated at least three times with similar  
573 results. Fig. S2B was performed twice. Data are represented as mean  $\pm$  SEM.

574            Statistical significance is from pooled data of the multiple independent experiments

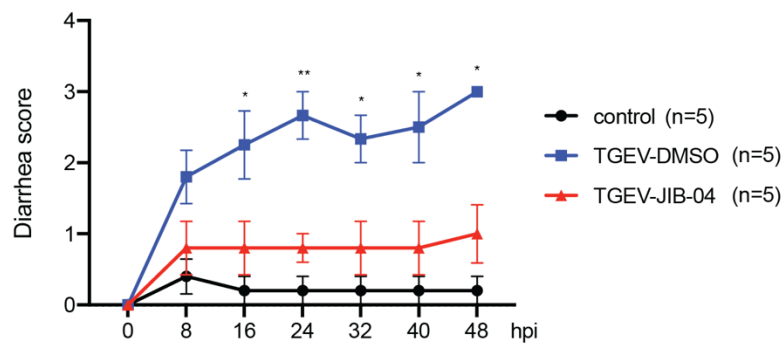
575            (\* $p \leq 0.05$ ; \*\* $p \leq 0.01$ ; \*\*\* $p \leq 0.001$ ).

576

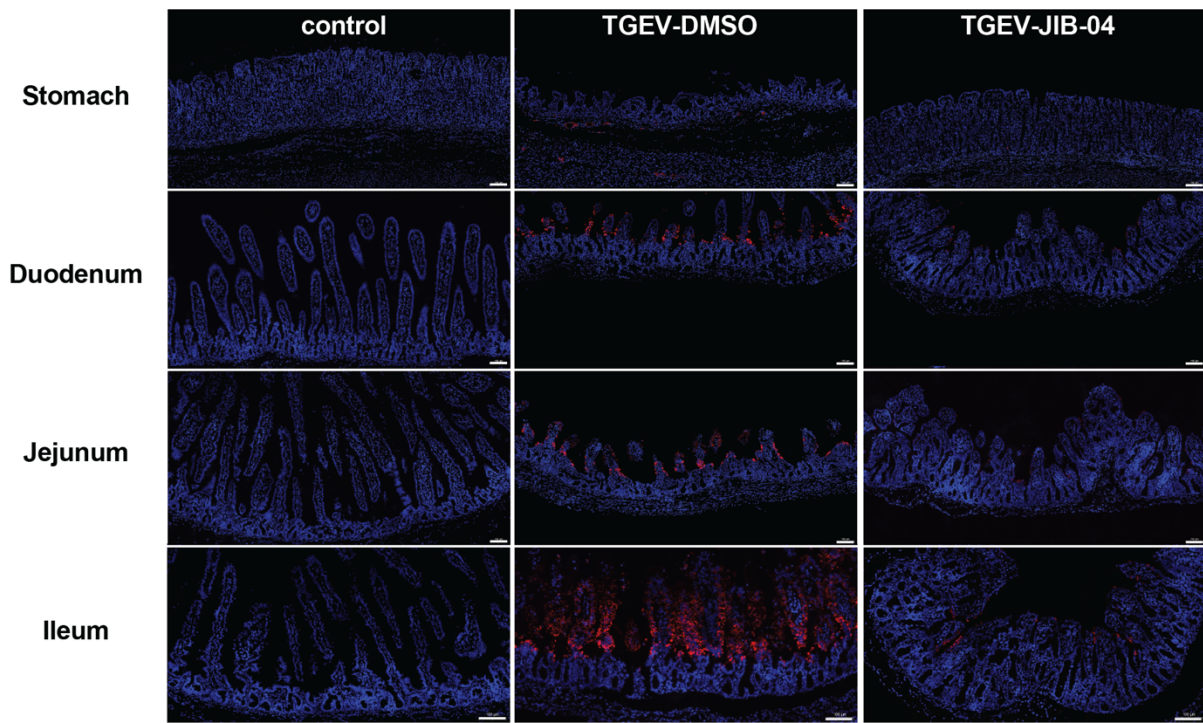
**A**



**B**



**C**



577  
578

579 **Fig. S4. JIB-04 reduces TGEV induced weight loss and pathogenesis**

580 (A) Weight of TGEV infected pigs with JIB-04 treatment in Fig. 4B. The body weight of  
581 individual animals was monitored every 24 h.

582 (B) Diarrhea occurrence in TGEV infected pigs with JIB-04 treatment in Fig. 4B.  
583 Diarrhea severity was scored for the fecal specimens of DMSO or JIB-04 treated,  
584 mock or TGEV infected animals every 8 h.

585 (C) Immunofluorescence staining of TGEV antigen in different GI tract sections from  
586 pigs sacrificed at 48 hpi. Blue: cell nuclei; red: TGEV nucleocapsid protein.  
587 Representative images of 3 animals. Scale bar, 100  $\mu$ m.

588

589 **REFERENCES**

590

- 591 Al-Beltagi, S., Preda, C. A., Goulding, L. V., James, J., Pu, J., Skinner, P., Jiang, Z., Wang, B. L., Yang,  
592 J., Banyard, A. C., Mellits, K. H., Gershkovich, P., Hayes, C. J., Nguyen-Van-Tam, J., Brown, I. H.,  
593 Liu, J. and Chang, K. C. (2021) 'Thapsigargin Is a Broad-Spectrum Inhibitor of Major Human  
594 Respiratory Viruses: Coronavirus, Respiratory Syncytial Virus and Influenza A Virus', *Viruses*, 13(2).  
595 Bayo, J., Tran, T. A., Wang, L., Pena-Llopis, S., Das, A. K. and Martinez, E. D. (2018) 'Jumonji  
596 Inhibitors Overcome Radioresistance in Cancer through Changes in H3K4 Methylation at Double-  
597 Strand Breaks', *Cell Rep*, 25(4), pp. 1040-1050 e5.  
598 Bolen, C. R., Ding, S., Robek, M. D. and Kleinstein, S. H. (2013) 'Dynamic expression profiling of  
599 Type I and Type III Interferon-stimulated hepatocytes reveals a stable hierarchy of gene  
600 expression', *Hepatology*.  
601 Case, J. B., Rothlauf, P. W., Chen, R. E., Liu, Z., Zhao, H., Kim, A. S., Bloyet, L. M., Zeng, Q., Tahan,  
602 S., Droit, L., Ilagan, M. X. G., Tartell, M. A., Amarasinghe, G., Henderson, J. P., Miersch, S., Ustav,  
603 M., Sidhu, S., Virgin, H. W., Wang, D., Ding, S., Corti, D., Theel, E. S., Fremont, D. H., Diamond, M.  
604 S. and Whelan, S. P. J. (2020) 'Neutralizing Antibody and Soluble ACE2 Inhibition of a Replication-  
605 Competent VSV-SARS-CoV-2 and a Clinical Isolate of SARS-CoV-2', *Cell Host Microbe*, 28(3), pp.  
606 475-485 e5.  
607 Cherry, S., Doukas, T., Armknecht, S., Whelan, S., Wang, H., Sarnow, P. and Perrimon, N. (2005)  
608 'Genome-wide RNAi screen reveals a specific sensitivity of IRES-containing RNA viruses to host  
609 translation inhibition', *Genes Dev*, 19(4), pp. 445-52.  
610 Dai, W., Zhang, B., Su, H., Li, J., Zhao, Y., Xie, X., Jin, Z., Liu, F., Li, C., Li, Y., Bai, F., Wang, H., Cheng,  
611 X., Cen, X., Hu, S., Yang, X., Wang, J., Liu, X., Xiao, G., Jiang, H., Rao, Z., Zhang, L. K., Xu, Y., Yang,  
612 H. and Liu, H. (2020) 'Structure-based design of antiviral drug candidates targeting the SARS-CoV-  
613 2 main protease', *Science*.  
614 Dalvi, M. P., Wang, L., Zhong, R., Kollipara, R. K., Park, H., Bayo, J., Yenerall, P., Zhou, Y., Timmons,  
615 B. C., Rodriguez-Canales, J., Behrens, C., Mino, B., Villalobos, P., Parra, E. R., Suraokar, M., Pataer,  
616 A., Swisher, S. G., Kalhor, N., Bhanu, N. V., Garcia, B. A., Heymach, J. V., Coombes, K., Xie, Y.,  
617 Girard, L., Gazdar, A. F., Kittler, R., Wistuba, II, Minna, J. D. and Martinez, E. D. (2017) 'Taxane-  
618 Platin-Resistant Lung Cancers Co-develop Hypersensitivity to JumonjiC Demethylase Inhibitors',  
619 *Cell Rep*, 19(8), pp. 1669-1684.  
620 Ding, S., Khoury-Hanold, W., Iwasaki, A. and Robek, M. D. (2014) 'Epigenetic reprogramming of  
621 the type III interferon response potentiates antiviral activity and suppresses tumor growth', *PLoS*  
622 *Biol*, 12(1), pp. e1001758.  
623 Ding, S., Zhu, S., Ren, L., Feng, N., Song, Y., Ge, X., Li, B., Flavell, R. A. and Greenberg, H. B. (2018)  
624 'Rotavirus VP3 targets MAVS for degradation to inhibit type III interferon expression in intestinal  
625 epithelial cells', *Elife*, 7.  
626 Dittmar, M., Lee, J. S., Whig, K., Segrist, E., Li, M., Kamalia, B., Castellana, L., Ayyanathan, K., Truitt,  
627 R., Yang, W., Jurado, K., Samby, K., Ramage, H., Schultz, D. and Cherry, S. (2021) 'Drug repurposing  
628 screens reveal cell-type specific entry pathways and FDA approved drugs active against SARS-  
629 Cov-2', *Cell Rep*.  
630 Gao, Y., Yan, L., Huang, Y., Liu, F., Zhao, Y., Cao, L., Wang, T., Sun, Q., Ming, Z., Zhang, L., Ge, J.,  
631 Zheng, L., Zhang, Y., Wang, H., Zhu, Y., Zhu, C., Hu, T., Hua, T., Zhang, B., Yang, X., Li, J., Yang, H.,

632 Liu, Z., Xu, W., Guddat, L. W., Wang, Q., Lou, Z. and Rao, Z. (2020) 'Structure of the RNA-  
633 dependent RNA polymerase from COVID-19 virus', *Science*, 368(6492), pp. 779-782.

634 Guo, R., Fan, B., Chang, X., Zhou, J., Zhao, Y., Shi, D., Yu, Z., He, K. and Li, B. (2020)  
635 'Characterization and evaluation of the pathogenicity of a natural recombinant transmissible  
636 gastroenteritis virus in China', *Virology*, 545, pp. 24-32.

637 Heiser, K., McLean, P. F., Davis, C. T., Fogelson, B., Gordon, H. B., Jacobson, P., Hurst, B., Miller,  
638 B., Alfa, R. W., Earnshaw, B. A., Victors, M. L., Chong, Y. T., Haque, I. S., Low, A. S. and Gibson, C.  
639 C. (2020) 'Identification of potential treatments for COVID-19 through artificial intelligence-  
640 enabled phenomic analysis of human cells infected with SARS-CoV-2', *bioRxiv*.

641 Hemeryck, A. and Belpaire, F. M. (2002) 'Selective serotonin reuptake inhibitors and cytochrome  
642 P-450 mediated drug-drug interactions: an update', *Curr Drug Metab*, 3(1), pp. 13-37.

643 Hoffmann, M., Kleine-Weber, H., Schroeder, S., Kruger, N., Herrler, T., Erichsen, S., Schiergens, T.  
644 S., Herrler, G., Wu, N. H., Nitsche, A., Muller, M. A., Drosten, C. and Pohlmann, S. (2020) 'SARS-  
645 CoV-2 Cell Entry Depends on ACE2 and TMPRSS2 and Is Blocked by a Clinically Proven Protease  
646 Inhibitor', *Cell*.

647 Hou, Y. J., Okuda, K., Edwards, C. E., Martinez, D. R., Asakura, T., Dinnon, K. H., 3rd, Kato, T., Lee,  
648 R. E., Yount, B. L., Mascenik, T. M., Chen, G., Olivier, K. N., Ghio, A., Tse, L. V., Leist, S. R., Gralinski,  
649 L. E., Schafer, A., Dang, H., Gilmore, R., Nakano, S., Sun, L., Fulcher, M. L., Livraghi-Butrico, A.,  
650 Nicely, N. I., Cameron, M., Cameron, C., Kelvin, D. J., de Silva, A., Margolis, D. M., Markmann, A.,  
651 Bartelt, L., Zumwalt, R., Martinez, F. J., Salvatore, S. P., Borczuk, A., Tata, P. R., Sontake, V., Kimple,  
652 A., Jaspers, I., O'Neal, W. K., Randell, S. H., Boucher, R. C. and Baric, R. S. (2020) 'SARS-CoV-2  
653 Reverse Genetics Reveals a Variable Infection Gradient in the Respiratory Tract', *Cell*.

654 Ianevski, A., He, L., Aittokallio, T. and Tang, J. (2020) 'SynergyFinder: a web application for  
655 analyzing drug combination dose-response matrix data', *Bioinformatics*, 36(8), pp. 2645.

656 Jin, Z., Du, X., Xu, Y., Deng, Y., Liu, M., Zhao, Y., Zhang, B., Li, X., Zhang, L., Peng, C., Duan, Y., Yu,  
657 J., Wang, L., Yang, K., Liu, F., Jiang, R., Yang, X., You, T., Liu, X., Yang, X., Bai, F., Liu, H., Liu, X.,  
658 Guddat, L. W., Xu, W., Xiao, G., Qin, C., Shi, Z., Jiang, H., Rao, Z. and Yang, H. (2020) 'Structure of  
659 M(pro) from SARS-CoV-2 and discovery of its inhibitors', *Nature*, 582(7811), pp. 289-293.

660 Kang, Y. L., Chou, Y. Y., Rothlauf, P. W., Liu, Z., Soh, T. K., Cureton, D., Case, J. B., Chen, R. E.,  
661 Diamond, M. S., Whelan, S. P. J. and Kirchhausen, T. (2020) 'Inhibition of PIKfyve kinase prevents  
662 infection by Zaire ebolavirus and SARS-CoV-2', *Proc Natl Acad Sci U S A*, 117(34), pp. 20803-20813.

663 Karchner, S. I., Franks, D. G., Powell, W. H. and Hahn, M. E. (2002) 'Regulatory interactions among  
664 three members of the vertebrate aryl hydrocarbon receptor family: AHR repressor, AHR1, and  
665 AHR2', *J Biol Chem*, 277(9), pp. 6949-59.

666 Kim, M. S., Cho, H. I., Yoon, H. J., Ahn, Y. H., Park, E. J., Jin, Y. H. and Jang, Y. K. (2018) 'JIB-04, A  
667 Small Molecule Histone Demethylase Inhibitor, Selectively Targets Colorectal Cancer Stem Cells  
668 by Inhibiting the Wnt/beta-Catenin Signaling Pathway', *Sci Rep*, 8(1), pp. 6611.

669 Kirchdoerfer, R. N. and Ward, A. B. (2019) 'Structure of the SARS-CoV nsp12 polymerase bound  
670 to nsp7 and nsp8 co-factors', *Nat Commun*, 10(1), pp. 2342.

671 Li, B., Ding, S., Feng, N., Mooney, N., Ooi, Y. S., Ren, L., Diep, J., Kelly, M. R., Yasukawa, L. L., Patton,  
672 J. T., Yamazaki, H., Shirao, T., Jackson, P. K. and Greenberg, H. B. (2017) 'Drebrin restricts rotavirus  
673 entry by inhibiting dynamin-mediated endocytosis', *Proc Natl Acad Sci U S A*, 114(18), pp. E3642-  
674 E3651.



675 Luo, L., Wang, S., Zhu, L., Fan, B., Liu, T., Wang, L., Zhao, P., Dang, Y., Sun, P., Chen, J., Zhang, Y.,  
676 Chang, X., Yu, Z., Wang, H., Guo, R., Li, B. and Zhang, K. (2019) 'Aminopeptidase N-null neonatal  
677 piglets are protected from transmissible gastroenteritis virus but not porcine epidemic diarrhea  
678 virus', *Sci Rep*, 9(1), pp. 13186.

679 Mirabelli, C., Wotring, J. W., Zhang, C. J., McCarty, S. M., Fursmidt, R., Frum, T., Kadambi, N. S.,  
680 Amin, A. T., O'Meara, T. R., Pretto, C. D., Spence, J. R., Huang, J., Alysandratos, K. D., Kotton, D.  
681 N., Handelman, S. K., Wobus, C. E., Weatherwax, K. J., Mashour, G. A., O'Meara, M. J. and Sexton,  
682 J. Z. (2020) 'Morphological Cell Profiling of SARS-CoV-2 Infection Identifies Drug Repurposing  
683 Candidates for COVID-19', *bioRxiv*.

684 Nguyen, H. L., Thai, N. Q., Truong, D. T. and Li, M. S. (2020) 'Remdesivir Strongly Binds to Both  
685 RNA-Dependent RNA Polymerase and Main Protease of SARS-CoV-2: Evidence from Molecular  
686 Simulations', *J Phys Chem B*, 124(50), pp. 11337-11348.

687 Ou, X., Liu, Y., Lei, X., Li, P., Mi, D., Ren, L., Guo, L., Guo, R., Chen, T., Hu, J., Xiang, Z., Mu, Z., Chen,  
688 X., Chen, J., Hu, K., Jin, Q., Wang, J. and Qian, Z. (2020) 'Characterization of spike glycoprotein of  
689 SARS-CoV-2 on virus entry and its immune cross-reactivity with SARS-CoV', *Nat Commun*, 11(1),  
690 pp. 1620.

691 Parrish, J. K., McCann, T. S., Sechler, M., Sobral, L. M., Ren, W., Jones, K. L., Tan, A. C. and Jedlicka,  
692 P. (2018) 'The Jumonji-domain histone demethylase inhibitor JIB-04 deregulates oncogenic  
693 programs and increases DNA damage in Ewing Sarcoma, resulting in impaired cell proliferation  
694 and survival, and reduced tumor growth', *Oncotarget*, 9(69), pp. 33110-33123.

695 Riva, L., Yuan, S., Yin, X., Martin-Sancho, L., Matsunaga, N., Pache, L., Burgstaller-Muehlbacher,  
696 S., De Jesus, P. D., Teriete, P., Hull, M. V., Chang, M. W., Chan, J. F., Cao, J., Poon, V. K., Herbert,  
697 K. M., Cheng, K., Nguyen, T. H., Rubanov, A., Pu, Y., Nguyen, C., Choi, A., Rathnasinghe, R.,  
698 Schotsaert, M., Miorin, L., Dejoze, M., Zwaka, T. P., Sit, K. Y., Martinez-Sobrido, L., Liu, W. C.,  
699 White, K. M., Chapman, M. E., Lendy, E. K., Glynn, R. J., Albrecht, R., Rupp, E., Mesecar, A. D.,  
700 Johnson, J. R., Benner, C., Sun, R., Schultz, P. G., Su, A. I., Garcia-Sastre, A., Chatterjee, A. K., Yuen,  
701 K. Y. and Chanda, S. K. (2020) 'Discovery of SARS-CoV-2 antiviral drugs through large-scale  
702 compound repurposing', *Nature*, 586(7827), pp. 113-119.

703 Saif, L. J. (2004) 'Animal coronavirus vaccines: lessons for SARS', *Dev Biol (Basel)*, 119, pp. 129-40.

704 Schneider, W. M., Luna, J. M., Hoffmann, H. H., Sanchez-Rivera, F. J., Leal, A. A., Ashbrook, A. W.,  
705 Le Pen, J., Ricardo-Lax, I., Michailidis, E., Peace, A., Stenzel, A. F., Lowe, S. W., MacDonald, M. R.,  
706 Rice, C. M. and Poirier, J. T. (2021) 'Genome-Scale Identification of SARS-CoV-2 and Pan-  
707 coronavirus Host Factor Networks', *Cell*, 184(1), pp. 120-132 e14.

708 Sheahan, T. P., Sims, A. C., Zhou, S., Graham, R. L., Pruijssers, A. J., Agostini, M. L., Leist, S. R.,  
709 Schafer, A., Dinno, K. H., 3rd, Stevens, L. J., Chappell, J. D., Lu, X., Hughes, T. M., George, A. S.,  
710 Hill, C. S., Montgomery, S. A., Brown, A. J., Bluemling, G. R., Natchus, M. G., Saindane, M.,  
711 Kolykhalov, A. A., Painter, G., Harcourt, J., Tamin, A., Thornburg, N. J., Swanstrom, R., Denison,  
712 M. R. and Baric, R. S. (2020) 'An orally bioavailable broad-spectrum antiviral inhibits SARS-CoV-2  
713 in human airway epithelial cell cultures and multiple coronaviruses in mice', *Sci Transl Med*,  
714 12(541).

715 Touret, F., Gilles, M., Barral, K., Nougaiere, A., van Helden, J., Decroly, E., de Lamballerie, X. and  
716 Coutard, B. (2020) 'In vitro screening of a FDA approved chemical library reveals potential  
717 inhibitors of SARS-CoV-2 replication', *Sci Rep*, 10(1), pp. 13093.

718 Wang, L., Chang, J., Varghese, D., Dellinger, M., Kumar, S., Best, A. M., Ruiz, J., Bruick, R., Pena-  
719 Llopis, S., Xu, J., Babinski, D. J., Frantz, D. E., Brekken, R. A., Quinn, A. M., Simeonov, A., Easmon,  
720 J. and Martinez, E. D. (2013) 'A small molecule modulates Jumonji histone demethylase activity  
721 and selectively inhibits cancer growth', *Nat Commun*, 4, pp. 2035.

722 Wang, M., Cao, R., Zhang, L., Yang, X., Liu, J., Xu, M., Shi, Z., Hu, Z., Zhong, W. and Xiao, G. (2020a)  
723 'Remdesivir and chloroquine effectively inhibit the recently emerged novel coronavirus (2019-  
724 nCoV) in vitro', *Cell Res*, 30(3), pp. 269-271.

725 Wang, R., Simoneau, C. R., Kulsuptrakul, J., Bouhaddou, M., Travisano, K. A., Hayashi, J. M.,  
726 Carlson-Stevermer, J., Zengel, J. R., Richards, C. M., Fozouni, P., Oki, J., Rodriguez, L., Joehnk, B.,  
727 Walcott, K., Holden, K., Sil, A., Carette, J. E., Krogan, N. J., Ott, M. and Puschnik, A. S. (2021)  
728 'Genetic Screens Identify Host Factors for SARS-CoV-2 and Common Cold Coronaviruses', *Cell*,  
729 184(1), pp. 106-119 e14.

730 Wang, X., Cao, R., Zhang, H., Liu, J., Xu, M., Hu, H., Li, Y., Zhao, L., Li, W., Sun, X., Yang, X., Shi, Z.,  
731 Deng, F., Hu, Z., Zhong, W. and Wang, M. (2020b) 'The anti-influenza virus drug, arbidol is an  
732 efficient inhibitor of SARS-CoV-2 in vitro', *Cell Discov*, 6, pp. 28.

733 Wei, J., Alfajaro, M. M., DeWeirdt, P. C., Hanna, R. E., Lu-Culligan, W. J., Cai, W. L., Strine, M. S.,  
734 Zhang, S. M., Graziano, V. R., Schmitz, C. O., Chen, J. S., Mankowski, M. C., Filler, R. B., Ravindra,  
735 N. G., Gasque, V., de Miguel, F. J., Patil, A., Chen, H., Oguntuyo, K. Y., Abriola, L., Surovtseva, Y.  
736 V., Orchard, R. C., Lee, B., Lindenbach, B. D., Politi, K., van Dijk, D., Kadoch, C., Simon, M. D., Yan,  
737 Q., Doench, J. G. and Wilen, C. B. (2021) 'Genome-wide CRISPR Screens Reveal Host Factors  
738 Critical for SARS-CoV-2 Infection', *Cell*, 184(1), pp. 76-91 e13.

739 Wu, F., Zhao, S., Yu, B., Chen, Y. M., Wang, W., Song, Z. G., Hu, Y., Tao, Z. W., Tian, J. H., Pei, Y. Y.,  
740 Yuan, M. L., Zhang, Y. L., Dai, F. H., Liu, Y., Wang, Q. M., Zheng, J. J., Xu, L., Holmes, E. C. and Zhang,  
741 Y. Z. (2020) 'A new coronavirus associated with human respiratory disease in China', *Nature*,  
742 579(7798), pp. 265-269.

743 Xie, X., Muruato, A., Lokugamage, K. G., Narayanan, K., Zhang, X., Zou, J., Liu, J., Schindewolf, C.,  
744 Bopp, N. E., Aguilar, P. V., Plante, K. S., Weaver, S. C., Makino, S., LeDuc, J. W., Menachery, V. D.  
745 and Shi, P. Y. (2020) 'An Infectious cDNA Clone of SARS-CoV-2', *Cell Host Microbe*.

746 Xu, M., Moresco, J. J., Chang, M., Mukim, A., Smith, D., Diedrich, J. K., Yates, J. R., 3rd and Jones,  
747 K. A. (2018) 'SHMT2 and the BRCC36/BRISC deubiquitinase regulate HIV-1 Tat K63-ubiquitylation  
748 and destruction by autophagy', *PLoS Pathog*, 14(5), pp. e1007071.

749 Yin, W., Mao, C., Luan, X., Shen, D. D., Shen, Q., Su, H., Wang, X., Zhou, F., Zhao, W., Gao, M.,  
750 Chang, S., Xie, Y. C., Tian, G., Jiang, H. W., Tao, S. C., Shen, J., Jiang, Y., Jiang, H., Xu, Y., Zhang, S.,  
751 Zhang, Y. and Xu, H. E. (2020) 'Structural basis for inhibition of the RNA-dependent RNA  
752 polymerase from SARS-CoV-2 by remdesivir', *Science*.

753 Zang, R., Case, J. B., Yutuc, E., Ma, X., Shen, S., Gomez Castro, M. F., Liu, Z., Zeng, Q., Zhao, H.,  
754 Son, J., Rothlauf, P. W., Kreutzberger, A. J. B., Hou, G., Zhang, H., Bose, S., Wang, X., Vahey, M. D.,  
755 Mani, K., Griffiths, W. J., Kirchhausen, T., Fremont, D. H., Guo, H., Diwan, A., Wang, Y., Diamond,  
756 M. S., Whelan, S. P. J. and Ding, S. (2020a) 'Cholesterol 25-hydroxylase suppresses SARS-CoV-2  
757 replication by blocking membrane fusion', *Proc Natl Acad Sci U S A*, 117(50), pp. 32105-32113.

758 Zang, R., Gomez Castro, M. F., McCune, B. T., Zeng, Q., Rothlauf, P. W., Sonnek, N. M., Liu, Z.,  
759 Brulois, K. F., Wang, X., Greenberg, H. B., Diamond, M. S., Ciorba, M. A., Whelan, S. P. J. and Ding,  
760 S. (2020b) 'TMPRSS2 and TMPRSS4 promote SARS-CoV-2 infection of human small intestinal  
761 enterocytes', *Sci Immunol*, 5(47).



762 Zhang, L., Lin, D., Sun, X., Curth, U., Drosten, C., Sauerhering, L., Becker, S., Rox, K. and Hilgenfeld,  
763 R. (2020) 'Crystal structure of SARS-CoV-2 main protease provides a basis for design of improved  
764 alpha-ketoamide inhibitors', *Science*, 368(6489), pp. 409-412.  
765 Zhou, P., Yang, X. L., Wang, X. G., Hu, B., Zhang, L., Zhang, W., Si, H. R., Zhu, Y., Li, B., Huang, C. L.,  
766 Chen, H. D., Chen, J., Luo, Y., Guo, H., Jiang, R. D., Liu, M. Q., Chen, Y., Shen, X. R., Wang, X., Zheng,  
767 X. S., Zhao, K., Chen, Q. J., Deng, F., Liu, L. L., Yan, B., Zhan, F. X., Wang, Y. Y., Xiao, G. F. and Shi,  
768 Z. L. (2020) 'A pneumonia outbreak associated with a new coronavirus of probable bat origin',  
769 *Nature*, 579(7798), pp. 270-273.  
770  
771

772 **Funding**

773

774 This study is supported by the National Institutes of Health (NIH) DDRCC grant P30  
775 DK052574, NIH grants K99/R00 AI135031 and R01 AI150796 and the COVID-19 Fast  
776 Grants Funding to S.D., NIH contracts and grants (75N93019C00062 and R01 AI127828)  
777 and the Defense Advanced Research Project Agency (HR001117S0019) to M.S.D., NIH  
778 grant U01 AI151810 to A.C.M.B., and unrestricted funds from Washington University  
779 School of Medicine and NIH grant R37 AI059371 to S.P.W. This study is partly funded by  
780 The Welch Foundation grant (I-1878) and NIH grant (R21AI139408) to E.D.M. The *in vivo*  
781 pig studies are supported by the Jiangsu Province Natural Sciences Foundation  
782 (BK20190003) and National Natural Science Foundation of China (31872481) to B.L.  
783 J.B.C. is supported by a Helen Hay Whitney Foundation postdoctoral fellowship.

784

785 **Author contributions**

786

787 J.S., Q.Z., R.Z., and S.D. designed, executed, and analyzed *in vitro* efficacy studies.  
788 M.F.G.C., H.P.K., and G.H. assisted with the RNA extraction and RT-qPCR analysis. Y.Z.  
789 performed the *in vitro* TGEV inhibition studies. Z.L. performed the flow cytometry analysis.  
790 L.C. wrote the algorithm that quantifies inhibitor screen results. P.W.R. and S.P.J.W.  
791 constructed the VSV-SARS-CoV-2 virus. E.D.M. provided JIB-04 Z-isomer. Q.Z., J.Z.,  
792 and R.G. propagated and titrated viruses. J.B.C. propagated and infected the clinical  
793 isolate of SARS-CoV-2. P.Y.S. provided the recombinant SARS-CoV-2 mNeonGreen  
794 virus. A.L.B propagated the mNeonGreen virus and designed the SARS-CoV-2 Taqman

795 probe. S.H., B.L., and S.D. designed the *in vivo* efficacy studies. S.H., J.Z., X.C., B.F.,  
796 and B.N., performed the *in vivo* TGEV infection experiments, dissected the animals and  
797 harvested tissues, and measured viral titers and cytokine mRNA levels. X.W., E.D.M.,  
798 S.P.J.W., M.S.D., A.C.M.B., B.L., and S.D. provided supervision and funding for the study.  
799 J.S. and S.D. wrote the manuscript with the input and edits from S.H., Q.Z., J.B.C., J.Z.,  
800 Z.L., M.F.G.C., H.P.K., G.H., S.P.J.W., M.S.D., A.C.M.B., and B.L.

801

## 802 **Competing interests**

803

804 The Boon laboratory has scientific research agreements with AI therapeutics, Greenlight  
805 Biosciences and Nano Targeting & Therapy Biopharma Inc. M.S.D. is a consultant for  
806 Inbios, Eli Lilly, Vir Biotechnology, NGM Biopharmaceuticals, and Emergent BioSolutions  
807 and on the Scientific Advisory Boards of Moderna and Immunome. The Diamond  
808 laboratory at Washington University School of Medicine has received unrelated  
809 sponsored research agreements from Moderna, Vir Biotechnology, and Emergent  
810 BioSolutions.

811

## 812 **Acknowledgements**

813

814 The authors thank Dr. Harry Greenberg (Stanford University, USA) and Dr. Bolívar A.  
815 Villacís-Bermeo (Guayaquil, Guayas, Ecuador) for constructive comments and  
816 arguments. We appreciate the assistance from Matthew Williams (Department of  
817 Molecular Microbiology Media and Glassware Facility) and Erica Lantelme (Department

818 of Pathology and Immunology, Flow Cytometry Core Facility). Cytation plate scanning  
819 was assisted by Zhou Huang (Department of Molecular Microbiology).

820

821 **Data and materials availability**

822

823 All raw data in the current study are available in Table S3 and Dataset S1. RNA-seq  
824 dataset has been deposited onto NCBI GEO (GSE156219).

825